USGS Award No. G18AP00078

Development of Deep Shear Wave Velocity Profiles at Seismic Stations in the Mississippi Embayment

Clinton Wood, Ph.D. P.E.[1] (PI)

Ashraf Kamal Himel[2]

University of Arkansas
Department of Civil Engineering
4190 Bell Engineering Center
Fayetteville, AR 72701
Phone: 479-575-6084
Fax: 479-575-7168
cmwood@uark.edu[1]
akhimel@uark.edu[2]

Project Period

August 1, 2018 – July 30, 2019

This material is based upon work supported by the U.S. Geological Survey under Grant No. G18AP00078. The views and conclusions contained in this document are those of the authors and should not be interpreted as representing the opinions or policies of the U.S. Geological Survey. Mention of trade names or commercial products does not constitute their endorsement by the U.S. Geological Survey.

Abstract

In this study, deep V_S profiles down to Paleozoic bedrock were developed at eight seismic stations and the Central United States Seismic Observatory (CUSSO), all situated in the Mississippi Embayment. A combination of active and passive surface wave methods (SWM) and horizontal to vertical spectral ratio measurements were used to estimate the shear wave velocity profile at each site. To validate the SWM, downhole measurements were made down to 425 m at the CUSSO site. The Vs profile developed using SWM and downhole at the CUSSO site agreed well, showing less than 1.0% difference in the time averaged shear wave velocity (Vs). The new Vs profiles at CUSSO provide an updated and more accurate Vs structure for the downhole array at the site. The Vs profile developed at each seismic station were compared to Vs profiles from the literature and those from the Central United States Seismic Velocity Model (CUSVM). Significant differences in the Vs profiles were observed between these sources; specifically, the Memphis sand layer (major impedance contrast in the embayment) was determined to be on average 81% deeper and 40% stiffer than the CUSVM model estimates. The developed V_S profiles in this study can be used to improve the accuracy of the current 3D velocity model of the embayment, and understand the potential site effects at CUSSO and other sites throughout the Mississippi Embayment.

Introduction

The deep sedimentary deposits of the Mississippi Embayment range from 477 m at New Madrid, Missouri to 987 m below Memphis, Tennessee (Van Arsdale and TenBrink 2000). The impact of this thick sediment layer on the ground motion is important but so far poorly understood (Hashash and Park 2001, Park and Hashash 2005). Past observations during historical earthquakes, such as the 1985 Mexico City, 1994 Northridge, and 2011 Christchurch, showed the strong influence of sediment thickness on the ground motion amplitude and frequency content (Hashash *et al.*, 2010, Mayoral *et al.*, 2019, Boore *et al.*, 2003, Bradley *et al.*, 2014). The Mississippi Embayment is situated in the New Madrid Seismic Zone (NMSZ), which has an estimated probability of 25 – 40% of a magnitude 6.0 or greater earthquake occurring within the next 50 years (Frankel *et al.*, 2009). To better understand the influence of sediment thickness on surface ground motion for site response analyses, quality shear wave velocity (V_S) profiles are critical (Bazzuro and Cornell 2004, Rathje *et al.*, 2010, Li and Assimaki 2010, Barani et al., 2013, Griffiths et al., 2016b, Teague and Cox 2016).

The Central United States Seismic Observatory (CUSSO) situated in southwestern Kentucky is a vertical seismic array. Previous studies from this array demonstrate a complex mixture of amplification/deamplification generated by the sedimentary deposits present in the Mississippi Embayment, which demands proper dynamic site characterization of the entire soil profile down to bedrock to fully understand the site effects on ground motions (Woolery *et al.*, 2016). The Mississippi Embayment has approximately 100 seismic stations to record the ground motion. These ground motions are the convolution of the input bedrock motion and the site effect. By conducting deconvolution of these ground motions, the bedrock input motion could be calculated (Idriss and Akky, 1979), which is essential to predict future ground motions in this area. A quality V_S profile is critical for the deconvolution process.

The V_S profile database for this region shows very few available site specific V_S profiles at seismic stations. Moreover, the majority of the V_S profiles available in the Embayment are only 30 – 60 m deep (Liu *et al.*, 1997, Street *et al.*, 2001, Street and Woolery, 2002). Rosenblad *et al.*, 2010 developed a set of deep Vs profiles in this region using surface wave methods, but these only range from 200 to 250 m deep. Woolery *et al.*, 2016 and Cramer *et al.*, 2004 used P-S suspension logging to develop deep V_S profiles at CUSSO (to bedrock) and Memphis light, gas and water well site (MLGW) (420 m), respectively. Romero and Rix, 2005 compiled V_S profiles from southern Tennessee, eastern Arkansas, and northwestern Missouri to form two reference deep V_S profiles for the lowlands and highlands of the embayment. These reference profiles have been used extensively for site response studies across the embayment. Gomberg *et al.*, 2003 showed that V_S profiles in the Mississippi Embayment are highly correlated with the lithology and could be extrapolated without direct measurements. Based on this philosophy, the Central United States Seismic Velocity Model (CUSVM) was developed using a significant number of boreholes and seismic refraction profiles (Ramirez-Guzman *et al.*, 2012).

To understand some of the variability in Vs profiles available in the embayment, a comparison between the V_S profile from Rosenblad *et al.*, 2010 site 5, the V_S profile from CUSVM at site 5, and Romero and Rix, 2005 lowland reference V_S profile is shown in Figure 1. In addition, a generalized profile from MLGW well 236 is included as a reference V_S profile (Cramer *et al.*,

2004). The MLGW 236 well is situated within 4 km of the Rosenblad *et al.*, 2010 site 5. Though the top 100 m of the profiles have a similar trend (increasing velocity with depth), an uncertainty of over 150 m/s (50% difference) is observed between the Vs profiles. Below 100 m, all the profiles start showing even more uncertainty. The Rosenblad *et al.*, 2010 and MLGW 236 have significant increases in V_S, making the CUSVM profile 15 – 50 % softer than the other profiles around 200 m. This comparison illustrates the uncertainty between the available Vs profiles in the embayment and highlights the need for additional Vs information.

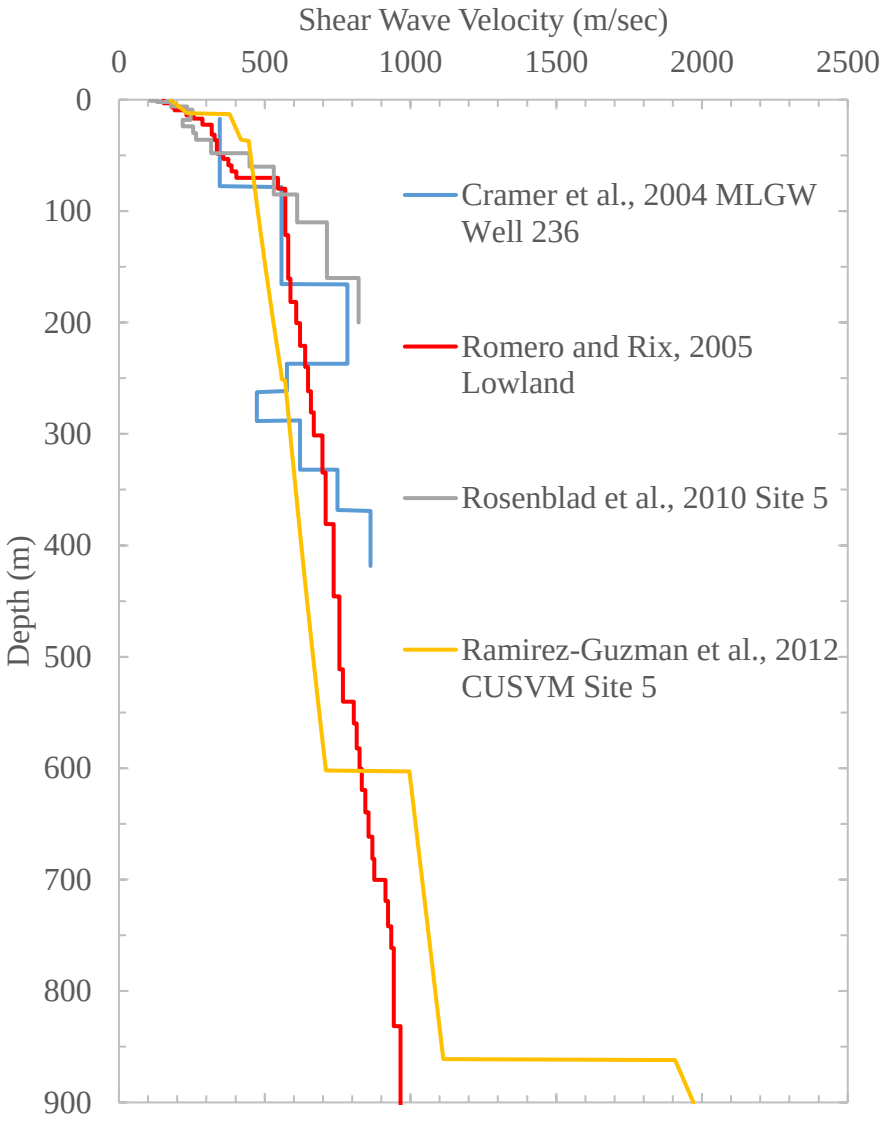

Figure 1. Comparison of Rosenblad *et al.*, 2010 Site 5 V_S profile with CUSVM Site 5, Romero and Rix, 2005 lowland and MLGW 236 V_S profiles.

The primary objective of this study is to develop deep shear wave velocity profiles down to the Paleozoic bedrock near eight seismic station and the CUSSO site in order to improve the available Vs information in this area. Surface wave testing was conducted at CUSSO and eight

seismic stations to develop these Vs profiles. In addition, downhole testing was conducted at the CUSSO site to validate the use of surface wave methods to develop deep Vs profiles in the embayment. The developed V_S profiles will be used to update the CUSVM, which presently demonstrates softer profiles at deeper depths than the measured V_S profiles.

Mississippi Embayment Geology

Deep, sedimentary, unconsolidated deposits characterize the Mississippi Embayment, which is generally described as a southward plunging syncline with an axis closely tracing the Mississippi river (Mento *et al.*, 1986). An idealized cross section of the Mississippi Embayment is shown in the Figure 2. The sedimentary deposit depth can extend from approximately 150 m in Jackson County, MO to 1100 m in Lee County, AR (Dart 1995). The bedrock found in the embayment is Knox Dolomite from the Paleozoic era (Cushing *et al.*, 1964), while the surface deposits are classified as Holocene or Pleistocene (Romero *et al.*, 2005). The Paleozoic bedrock and the Memphis sand are the two main impedance contrasts in the Mississippi Embayment (Rosenblad *et al.*, 2010). The alluvial surface deposits have a low V_S of 193 ± 14 m/sec compared with the Memphis sand and the Paleozoic bedrock units, which have V_S of 685 ± 83 m/sec (Rosenblad *et al*. 2010) and 2000 - 3400 m/sec (Cramer 2006), respectively.

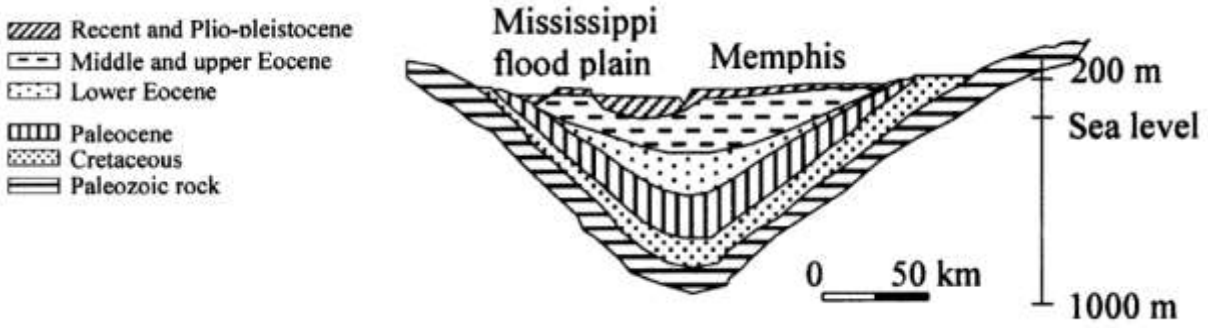

Figure 2. Idealized cross section of the Mississippi Embayment (Hashash and Park, 2001)

Quaternary, Upper Tertiary, Lower to Middle Claiborne, Paleocene, Cretaceous and Paleozoic era bedrock are the main constituents of the Mississippi Embayment's geology (Ramirez-Guzman *et al*. 2012). In the uppermost Quaternary layer, the surface deposits are classified as Holocene or Pleistocene (Romero *et al*. 2005). Holocene deposits are mainly found in the alluvial plains of the Mississippi River floodplain, also known as the lowlands and Pleistocene deposits are found further east on the highlands (Romero *et al*. 2005). As shown in Figure 3, the lowlands are situated to the west of the Mississippi River and the highlands are situated to the east.

The Upper Tertiary layer is situated below the Quaternary layer, consisting of the Jackson formation and the upper Claiborne group. The Jackson formation consists of clay, silt, sand and lignite (Brahana *et al*. 1987), whereas the upper Claiborne includes Cockfield and Cook Mountain formation, characterized by silts and clay (Van Arsdale *et al*. 2000).

Lower to Middle Claiborne group (LMC) is found below the Upper Tertiary layer. The Memphis sand unit is a part of the LMC, which is a very fine to coarse grained and light gray-white sand (Van Arsdale *et al*. 2000). Memphis sand, also known as the "500 feet sand" (Romero *et al*. 2005), is the principle aquifer for the Memphis area. This unit can be 164 – 292 m thick and is approximately 300 m deep in the Memphis area (Brahana *et al*., 1987).

The Paleocene layer contains the Wilcox and Midway groups, which are made up of several formations. The Wilcox group contains the Flour Island Formation, Fort Pillow Sand and Old Breastworks formation. The Flour Island Formation consists of alternating layers of silt, clay, and medium to light gray sand. The Fort Pillow Sand is thick, fine to coarse grained, marine sand and is 64 m thick in Shelby County, Tennessee (Van Arsdale and TenBrink, 2000). The Old Breastworks Formation is 95 m thick clayey silt beneath Shelby County, Tennessee (Hosman, 1996). The Midway group contains the Porters Creek Clay Formation (thick body clay) and Clayton Formation (clay, sand, and minor limestone) (Brahana *et al.,* 1987). The Midway group is composed primarily of marine clay and thins from 160m near Memphis to 100 m near New Madrid, Missouri (Van Arsdale and TenBrink 2000).

Just above the bedrock layer is the Cretaceous and Mesocenozoic layer. These layers contain several forms of clays and sands, and consist of the McNairy Sand layer, the Demopolis Formation, and the Coffee Formation. The McNairy Sand layer indicates the top of the layer. It is composed of thick calcareous marine sand. It thins from 130 m thick at Shelby County to 95m thick at New Madrid. The Demopolis Formation lies below the McNairy Sand. It is a calcareous marine clay (Van Arsdale and TenBrink 2000). Below the Demopolis Formation is the Coffee Formation, which contains a well-sorted, loose-to-friable sand that is interbedded with thin carbonaceous clays (Russell *et al.,* 1982). The Paleozoic bedrock layer signifies the basement of the Mississippi Embayment deposits and is primarily made up of white to dark-gray, fine to coarse crystalline dolomite (Van Arsdale and TenBrink 2000).

Site Location and Testing Methodology

The nine seismic station sites characterized in this project are shown in Figure 3. The majority of the sites are situated on the lowland part of the Mississippi Embayment, generally within close proximity of the Lowland-Highland boundary. Only the TUMT and LNXT sites are situated on the highland portion of the embayment. Dynamic site characterization was conducted using surface wave methods at each site, while both surface wave methods and downhole seismic testing were conducted at the CUSSO site. The location of the sites are tabulated in Table 1. Bedrock depth for each site in Table 1 (except CUSSO) are from Ramirez-Guzman *et al.*, 2012. The bedrock depth for CUSSO is from Woolery *et al.*, 2016.

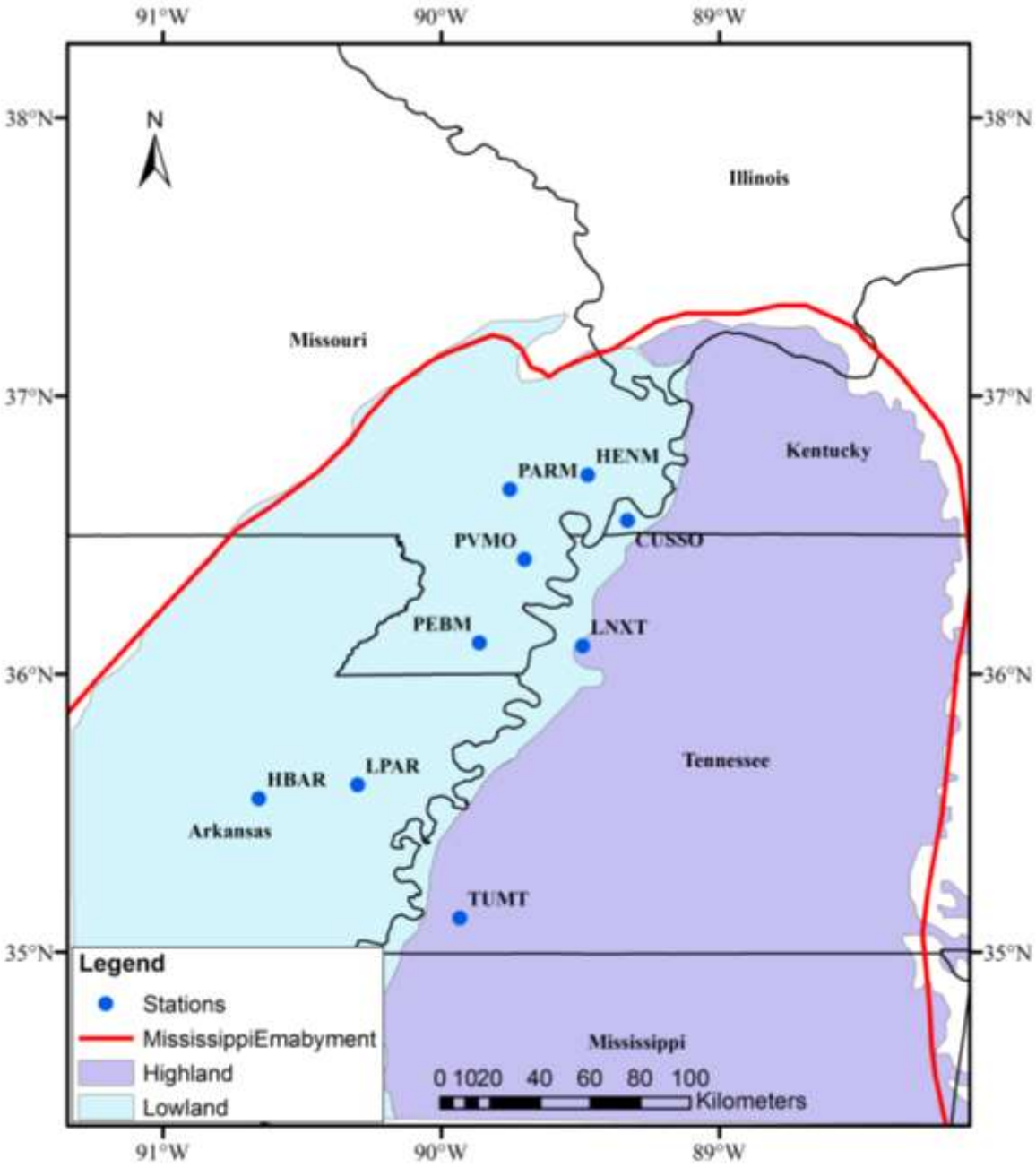

Figure 3. Map of the Mississippi Embayment showing the seismic stations characterized in this study, and the highland and lowland area in the Embayment.

Table 1. Site locations and bedrock depth of seismic stations characterized in this study (Ramirez-Guzman *et al.*, 2012, Woolery *et al.*, 2016).

Station Name	Latitude	Longitude	Bedrock Depth (m)
PARM	36.664	-89.752	427
HENM	36.716	-89.472	450
CUSSO	36.552	-89.329	585
PVMO	36.413	-89.699	591
HBAR	35.553	-90.654	754
PEBM	36.113	-89.862	764
LPAR	35.602	-90.300	840
LNXT	36.101	-89.491	845
TUMT	35.123	-89.933	923

Non-Invasive Testing

Deep shear wave velocity profiles were developed at each seismic station in Table 1 using a combination of active-source and passive source surface wave methods. Active source multichannel analysis of surface wave (MASW) (Park *et al.*, 1999) was used at each site to characterize the near surface materials, while passive source microtremor array measurements (MAM) (Aki 1957, Tokimatsu 1997) were used to characterize the deeper materials. In Figure 4, a general testing layout for surface wave measurement is shown for the HENM site.

For each site, MASW was conducted using a linear array of 24, 4.5 Hz geophones with 2 m receiver spacing (46 m array length). Both Rayleigh and Love surface wave data were recorded using vertical and horizontal geophones, respectively. Rayleigh and Love waves were generated by vertical and horizontal strikes from a 5.4 kg sledgehammer, respectively. Multiple source offsets of 5, 10, 20, and 40 m from the first geophone were used to estimate uncertainty and minimize near-field effects. Ten sledgehammer blows were stacked at each source offset to improve the signal-to-noise ratio. Using the vertical MASW geophone array, P-wave refraction was conducted at each site using an offset of 2 m from the first geophone. Ten vertical sledgehammer blows were staked at the offset. A general layout of the MASW and P-wave refraction arrays are shown in Figure 5.

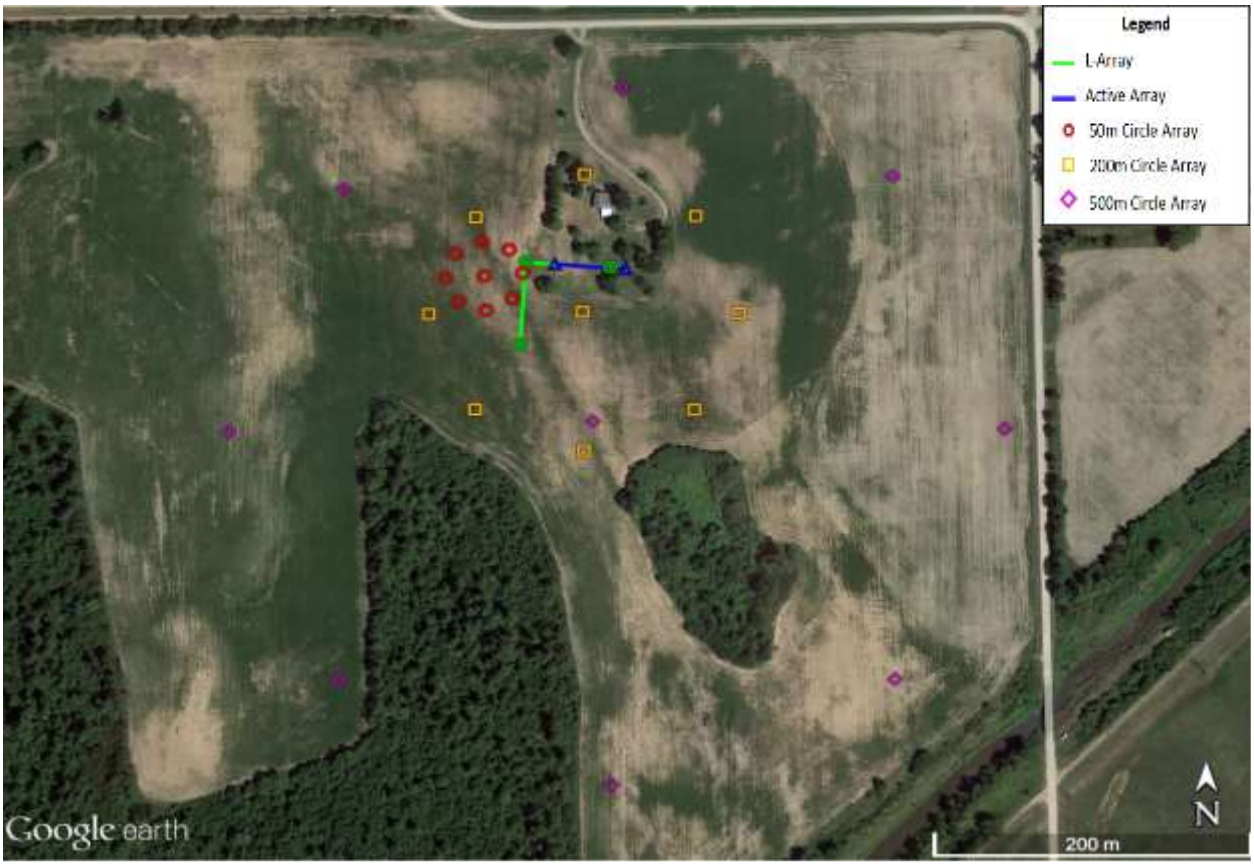

Figure 4: Surface wave testing layout shown for the HENM site. In this figure, the MASW active array, 50 m, 200 m and 500 m circular arrays, and L-array are shown.

Figure 5. A general testing methodology for MASW and P-wave refraction is shown. In (a), linear array of vertical and horizontal geophones is shown. In (b) and (c), Rayleigh and Love wave generation, respectively from vertical and horizontal sledgehammer impacts are shown.

The MAM measurements were carried out using circular and L-shaped arrays. Both 2D arrays are capable of determining the orientation of wave propagation from unknown sources. The circular array MAM measurements utilized nine three-component Trillium Compact, 20-second broadband seismometers. In each circular array arrangement, eight seismometers were uniformly distributed on the circumference, while the ninth seismometer was placed on the center. Circular arrays of 50 m, 200 m, and 500 m diameter were used at all sites. Each seismometers was placed on a leveling cradle which was held firm in the ground by 10 cm long spikes. A bucket was placed over each seismometer to reduce noise produced by wind. A typical installation process for the seismometers are shown in Figure 6. Ambient noise was typically recorded for 30 min, 1 hour and 1.5 hour for the 50 m, 200 m, and 500 m circular arrays, respectively. A Nanometrics Centaur digitizer was used for recording the data. This digitizer uses a GPS timing system (included with the unit) to synchronize between the stations (Nanometrics 2017). After deployment, the location of each seismometer was recorded using a Trimble Geo 7x centimeter accuracy GPS unit with a Zephyr 2 external antenna.

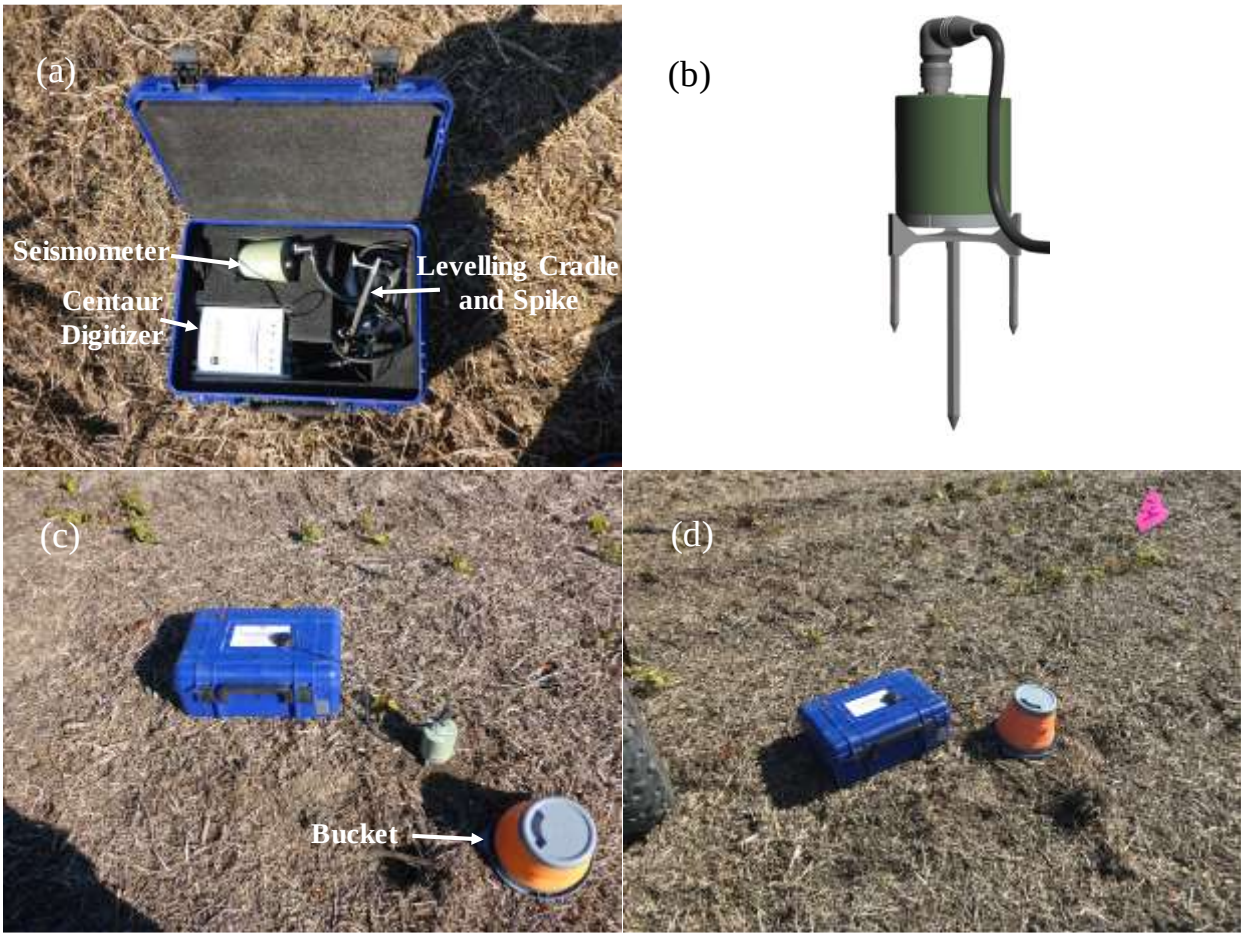

Figure 6. A typical seismometer installation process used during testing. (a)Nanometrics Trillium Compact seismometer with Centaur digitizer, leveling cradle and spikes for installation are shown. (b) A schematic diagram of the seismometer, placed on levelling cradle and spikes. (c) In the field, a seismometer is leveled on the leveling cradle and firmly attached with the soil using the spikes. (d) A bucket is placed over the seismometer to reduce noise caused by wind.

The L-array MAM measurements were carried out using 24, 4.5 Hz vertical geophones. An equal receiver spacing of 5 m was used, which resulted in an L-array with dimensions of 55 m x 60 m. All sites, except the LNXT site have the same L-array geometric configuration. Due to space constraints, a 4 m receiver spacing, which resulted in a 24 m x 68 m L-array was used for the LNXT site. Microtremors were recorded for approximately 1 hour at each site.

The passive data recorded by the seismometers in the MAM measurements were also used for the Horizontal-to Vertical Spectral Ratio (HVSR) measurements at each site.

More information regarding the measurements made at each site can be found on designsafe at https://doi.org/10.17603/ds2-be10-q668.

Invasive Testing

Downhole seismic testing was conducted at the CUSSO site in two stages: preliminary shallow testing to 115 m and followed by deep testing to 425 m. Shallow and deep downhole testing was conducted in the 259 meter and 587 meter deep boreholes, respectively. Each borehole used 4" steel casing. Field data for shallow testing was collected in general accordance with ASTM D7400-08 "Standard Test Methods for Downhole Seismic Testing". The receiver used for testing was a Geostuff BHG-3 wall-lock borehole geophone system. Due to the steel casing, the orientation mechanism in the BHG-3 could not be utilized during testing. For each downhole test, the water level in the borehole was lowered to approximately 30 m prior to testing.

For shallow testing, a vehicle-on-beam traction source and steel strike plate were offset from the borehole 3.05 meters (see Figure 7). The traction plank was oriented East-West and held in firm contact with the ground by a pickup. Downward propagating P-waves were generated by vertical sledgehammer blows on a steel strike plate. Downward propagating, horizontally polarized shear waves were generated by horizontal blows on the traction beams. Blows were made on either end of the beam to produce "positive" and "negative" polarity shear waves which are used in the analysis to aid in identifying the first arrival. The sledge hammer was equipped with a sensor that triggers the recording process upon impact with the beam. Five sledgehammer blows were stacked at each depth to increase the signal-to-noise ratio. During testing, the trigger signal is constantly monitored to assure consistent measurements are made. A Data Physics Quattro dynamic signal analyzer was used to record waveforms during testing. Testing was performed from the top-down and started at 0.75 m below the ground surface. Sampling intervals of 0.75 m were used near the ground surface (i.e., to a depth of 15 m), while sampling intervals of 1.5 m were used after that depth.

For deep testing, an Industrial Vehicles International (IVI) T-15000 Vibroseis was utilized as the shear wave source (see Figure 8). The Vibroseis was offset from the borehole by 3.05 m and the reaction mass was oriented perpendicular from the borehole to generate horizontally polarized shear waves. An 8 sec. sinusoidal sweep from 20-80 Hz was used during testing with 3-5 averages used at each depth. A Data Physics Mobilyzer dynamic signal analyzer was used to record waveforms during testing. Testing was performed from the top-down and started at 3 m below the ground surface. A sampling interval of 3 m was used to the final depth of 425 m. For more information regarding the downhole testing, please see the archived data at https://doi.org/10.17603/ds2-be10-q668.

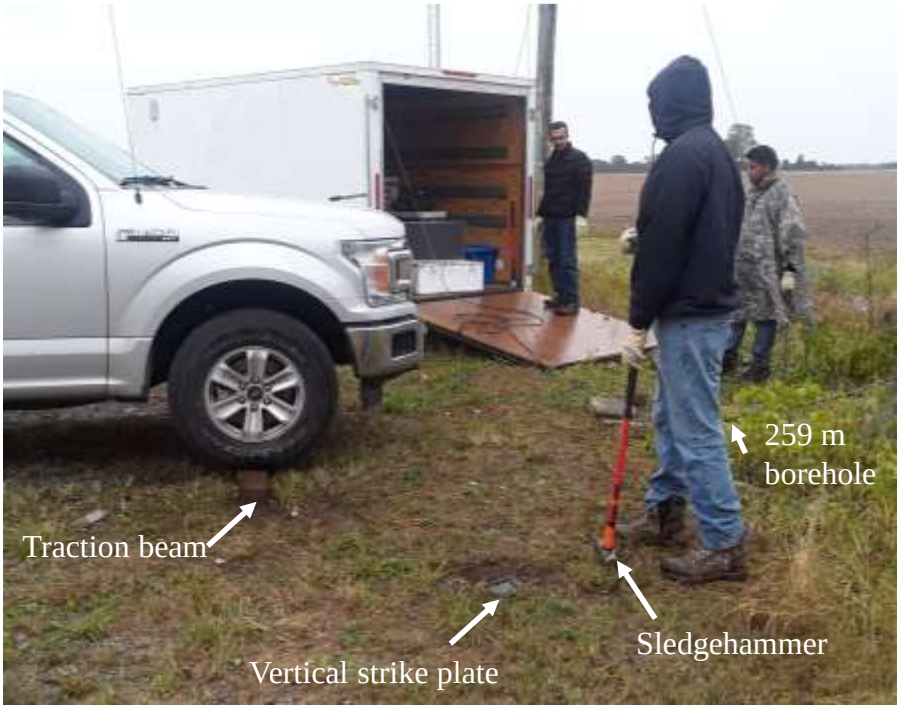

Figure 7: Shallow downhole equipment layout for CUSSO site at 259 m borehole.

Figure 8: Deep downhole equipment layout for CUSSO site at 587 m borehole.

Data Processing

Non-Invasive

The active and passive surface wave data collected from the field were processed to develop the experimental dispersion data, HVSR and P-wave refraction results. This dispersion data and HSVR information are used to conduct a joint inversion to solve for the V_S profile at each site. The P-wave refraction data are analyzed to estimate the approximate water table depth. The data processing steps are as follows:

i. Dispersion Processing
ii. HVSR Processing
iii. P-wave Refraction Processing
iv. Inversion

(i) Dispersion Processing: The MASW data (both Rayleigh and Love) were processed using the Frequency Domain Beamformer (FDBF) method in combination with the multiple-source offset technique (Zywicki, 1999, Cox and Wood 2011). For each site, the dispersion curves for each source offset were combined to form a single composite experimental dispersion curve. In the composite curve, all identifiable near-field data (below approximately 5 – 7 Hz depending on the site) and effective mode data were removed. After this process, only the fundamental dispersion data were used to develop a final composite experimental dispersion curve with associate uncertainty. Figure 9 demonstrates a typical process for the near-field effect and higher/effective mode data removal for MASW.

Rayleigh and Love wave dispersion data was estimated from the circular array MAM measurements using the High Resolution Frequency Wave Number (HRFK) method (Capon 1969), while only Rayleigh wave dispersion data was estimated using the Modified Spatial Auto-Correlation (MSPAC) method (Bettig *et al.*, 2001). For the HRFK method, the Rayleigh wave dispersion data was obtained from the vertical component of the seismometers while the Love wave data was obtained by rotating the two horizontal components to create a component perpendicular to the identified direction of Rayleigh wave propagation. For both Rayleigh and Love wave processing, the recorded data were divided into 20 to 40, 180 second time windows to ensure a sufficient number of cycles for the frequency range of interest. For each time window, peak wavenumber pairs were selected at 125 frequency samples spaced on a log distribution between 0.1 and 20 Hz. Dispersion points outside of the array resolution limits were removed (Wathelet *et al.*, 2008). Each of the circular arrays was processed independently and then combined to form a composite HRFK dispersion curve. In Figure 10, a composite HRFK dispersion plot is shown for the three circular arrays. The mean phase velocity and standard deviation at each frequency bin are calculated given the data from each array and window.

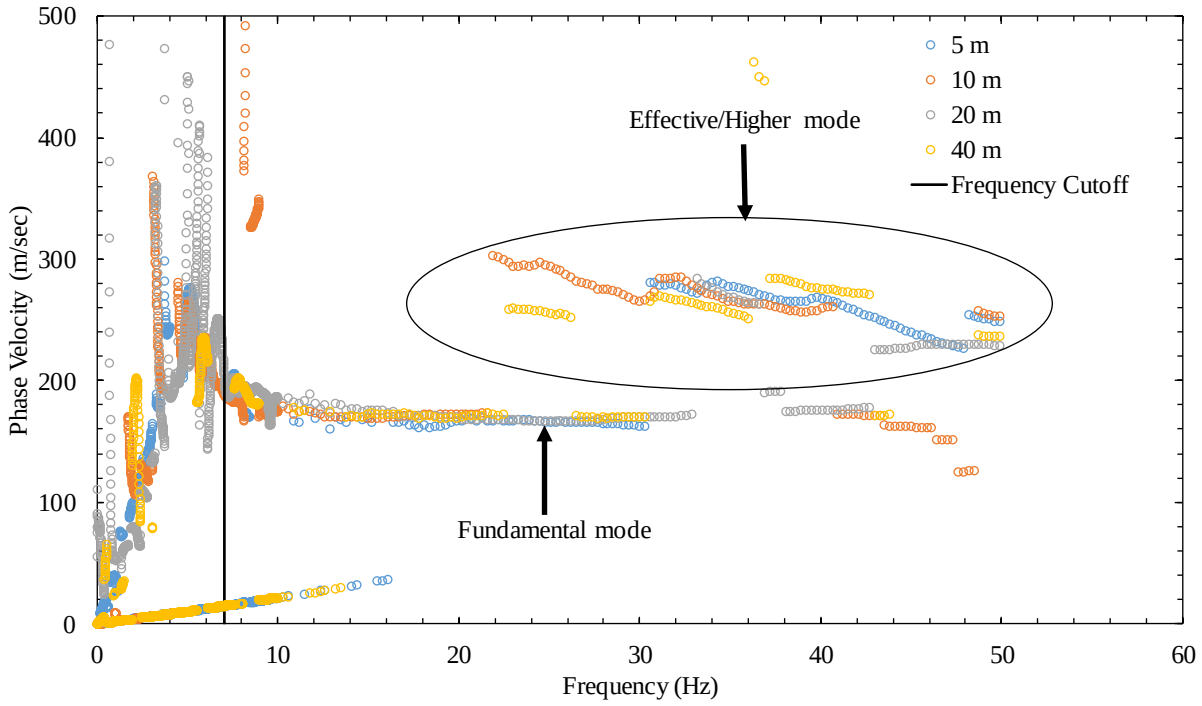

Figure 9. Dispersion data from MASW for CUSSO. Dispersion data from the four source offsets (5 m, 10 m, 20 m, and 40 m) were combined to develop the composite dispersion plot for MASW. A cutoff frequency of approximately 7 Hz was used to eliminate the data where the uncertainty grows to large and potential near-field effect may effect that data. The effective/higher mode data were also eliminated.

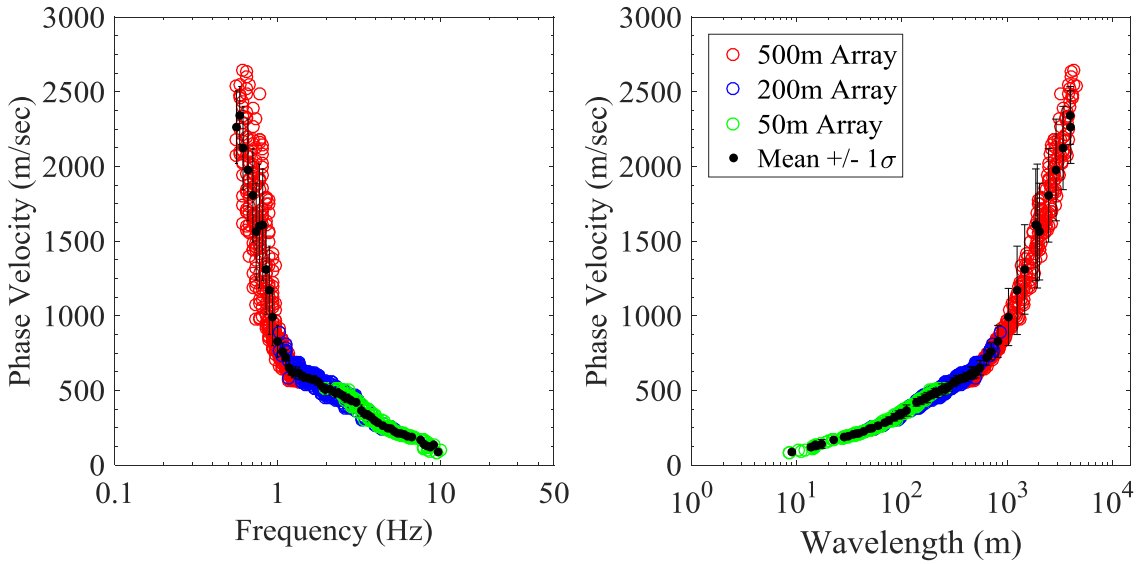

Figure 10. Rayleigh wave dispersion data processed by the HRFK method independently for 50 m, 200 m, and 500 m circular array MAM measurements is shown for the site LPAR. Dispersion data from all three circular arrays are combined together to form a composite HRFK dispersion plot. The mean phase velocity (shown with black dots) and standard deviation for each frequency bin are calculated from the data.

In the MSPAC method, the receiver pairs are divided into sets of circular sub-arrays or rings. The recorded MAM data are divided into 180 second time windows and for each time window, the auto-correlation values are calculated for individual rings for 125 frequency bins spaced on a log scale from 0.1 to 10 Hz. For each ring, an average autocorrelation value is calculated. Later, manual selection of the middle (average), upper and lower bound phase velocities are made from the histograms produced from the auto-correlation values. This manual picking is done separately for each circular array and unlike the HRFKs averaged dispersion curves, results in individual dispersion curves for each circular array.

Finally, all the dispersion curves produced by different methods are combined together to form a composite experimental dispersion curve for Rayleigh and Love surface wave data (Park *et al.*, 2005, Martin *et al.*, 2005, Foti *et al.*, 2007). Before combining the dispersion curves, each curves were processed to eliminate the effective mode data and outlying phase velocity points. Individual curves were also compared together to reduce the mode transition and near field effects (Wood *et al.*, 2014). An example composite Rayleigh dispersion curve is shown in Figure 11.

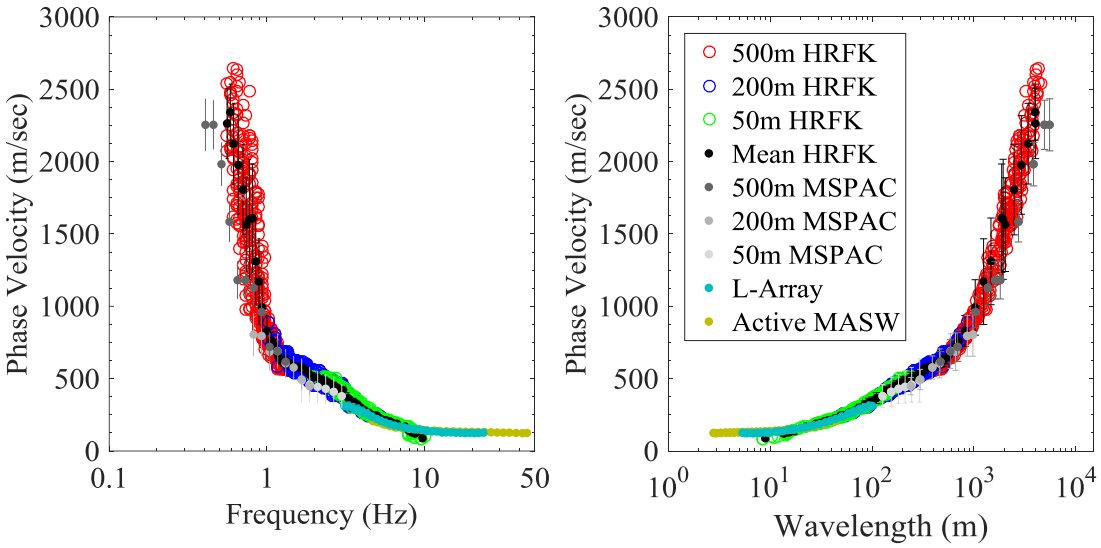

Figure 11. Experimental composite dispersion curve for the LPAR site (Rayleigh wave only).

(ii) HVSR Processing: The ambient data collected with the circular arrays were used to compute the HVSR for the nine individual seismometers in each array. Time records were divided into 20 to 40, 180 second time windows and transformed to the frequency domain using a Fourier transformation. The geometric mean of the horizontal components were used to calculate the horizontal to vertical spectral ratio for each time window. The HVSR peak of all time windows of a record were used to produce an average peak with associate standard deviation. The average peak from all nine sensors are then combined to determine a single HVSR peak frequency with associate uncertainty for the site. General guidelines established by the SESAME projects were followed for the HVSR processing (SESAME 2004). The peaks in the HVSR curves represent velocity contrast where a stiffer layer underlies a softer layer. Typically, the peak at the lowest frequency represents the fundamental frequency of the site. An example HVSR curve from the CUSSO site, along with its first peak are shown in Figure 12.

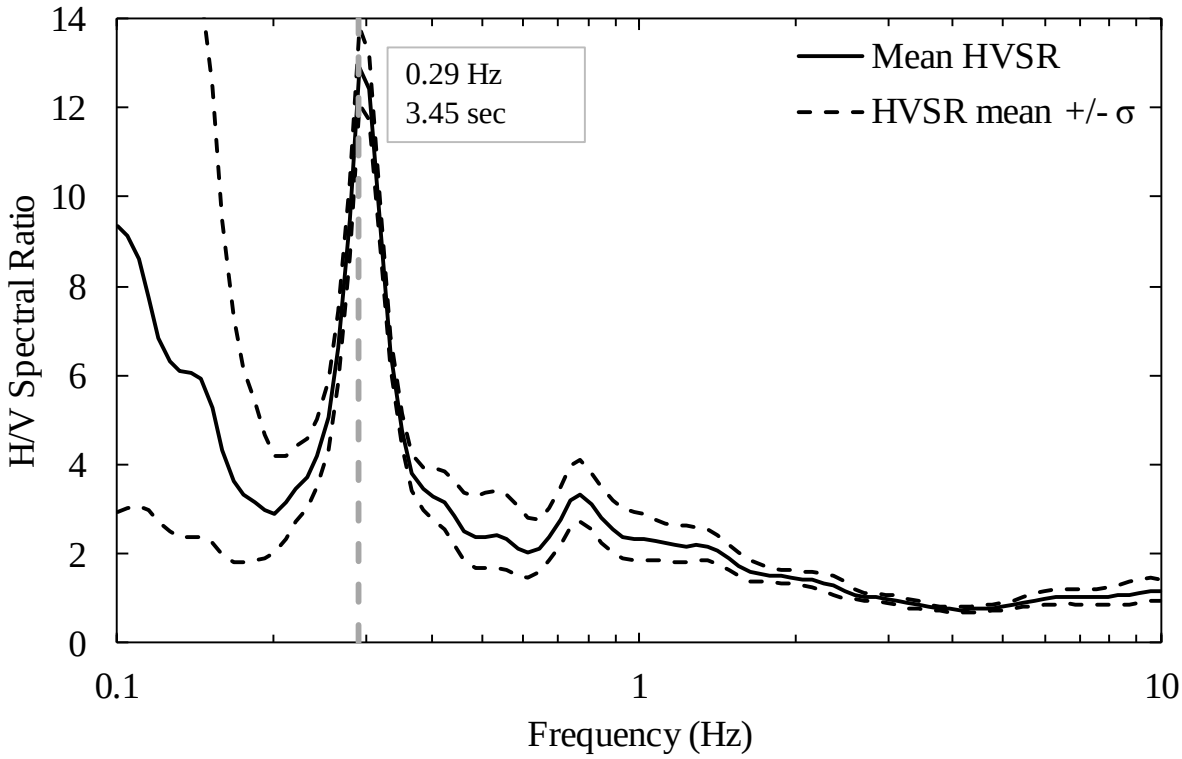

Figure 12. An example HVSR plot from the CUSSO site, where the natural frequency of the site was 0.29 Hz.

(iii) P-wave Refraction: The P-wave refraction data was processed following Redpath (1973). Time series were processed to identify the P-wave arrival, at each receiver offset, as a function of time. These time records were analyzed in a 'waterfall' plot as shown in Figure 13. The red circles indicate the picks of the P-wave arrivals and the black lines are linear fits through the points at what appear to be layers with the intersection of these lines representing the location of the layer interface. The slopes of the lines are equivalent to the P-wave velocity (V_p) of the layers (e.g., upper soil layer and the water table). The critical distance and intercept time methods are used to estimate the depth to the water table (line of saturation), which is approximately 6.5 meters deep at this example site.

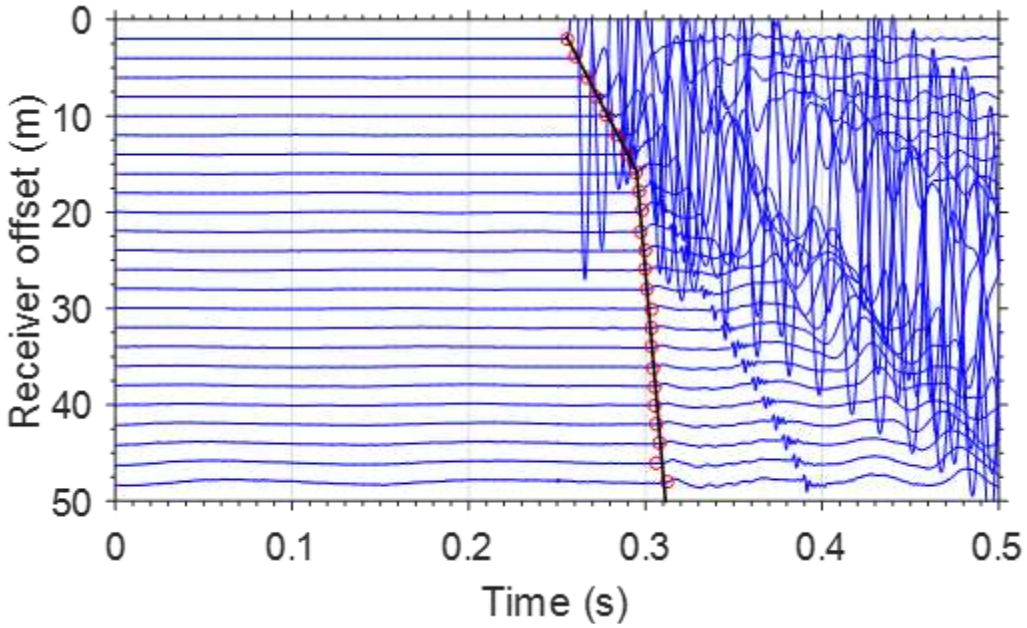

Figure 13: An example of a waterfall plot of P-wave arrivals at each receiver. The red circles show the picks of the P-wave arrivals and the black lines are linear fits through the points at what appear to be layers with the intersection of these lines representing the location of the layer interface.

(iv) Inversion: A joint inversion of the composite experimental dispersion curves and site period was conducted to obtain the shear wave velocity profiles using the Geopsy software package Dinver (Wathelet *et al*., 2008). Dinver utilizes a neighborhood algorithm, which generates theoretical dispersion curves and ellipticity curves for trial V_S profiles constrained by the user provided parameters. The parameters include ranges of shear wave velocity, P-wave velocity, Poisson's ratio, density and the number of layers. The V_S profiles generated within these constraints are used to create corresponding theoretical dispersion curves and ellipticity curves using a forward model (Thomson 1950, Haskell 1953, Dunkin 1965, Knopoff 1964). The theoretical dispersion curves are compared with the experimental dispersion curves and the HVSR peak is compared to the peak of the ellipticity curve. An overall 'closeness' between these experimental and theoretical results are computed, which is quantified as a misfit. Misfit values less than one indicate that the theoretical dispersion curve and ellipticity peak primarily fit within one standard deviation of the experimental dispersion curve and ellipticity peak. The neighborhood algorithm attempts to minimize this misfit at each frequency bin along the dispersion curve. During this iterative process, effective and higher modes are also identified manually by comparing the theoretical dispersion curves and experimental data after each inversion run. The higher mode data, which have higher phase velocity at the same frequency as the fundamental mode data are identified. The effective mode data typically shifts from one mode of data to another mode and are detected by their deviation from one propagation mode's general trend to another mode. Since Dinver cannot utilize the effective modes, these data are eliminated after detection. An example of effective and higher mode data detection is shown in Figure 14. In this figure, experimental Rayleigh wave dispersion data developed using active MASW, circular passive HRFK and MSPAC, and L-array are shown along with the calculated minimum misfit theoretical dispersion curve. The active MASW, L-Array, and HRFK each resolve the fundamental mode at frequencies

greater than 1.0 Hz. However, below 1.0 Hz, the HRFK data transitions from the fundamental mode to an effective mode, then to the first higher mode. The MSPAC data, on the other hand, is identified as fundamental mode for its entire frequency band from 0.5 – 1.5 Hz. The identification of the mode of propagation of each dispersion point is always an iterative process requiring comparison of datasets and inversion runs. After identifying the mode of all dispersion points, the effective mode data is eliminated, but the higher mode data are assigned with their proper modes and used in the inversion process.

For this study, a broad range for parameters were utilized to find the best solution. A priori knowledge from the literature were applied for developing the parameters (Ramírez-Guzmán *et al*., 2012, Lin *et al*., 2014, Romero and Rix 2005, Rosenblad *et al*., 2010, Woolery *et al*., 2016). Vs ranges for each layer were defined based on Vs from the CUSVM and reference curves from Lin et al. (2014). Poisson's ratio was allowed to vary between 0.25-0.35 for soils above the water table. Poisson's ratio for soils below the water table (which was identified based on P-wave refraction results) was based on a Vp of 1500 m/s in the near surface, however at depths where Vs was greater than 750 m/s, Vp was allowed to increase beyond 1500 m/s to constrain Poisson's ratio between the range of 0.25-0.35 which is typical for dense sand and gravel layers present at these depths (Coduto 1999). Most importantly, the bedrock depths in the inversion processing were constrained using the bedrock depth information from the CUSVM (Ramirez-Guzman *et al.*, 2012).

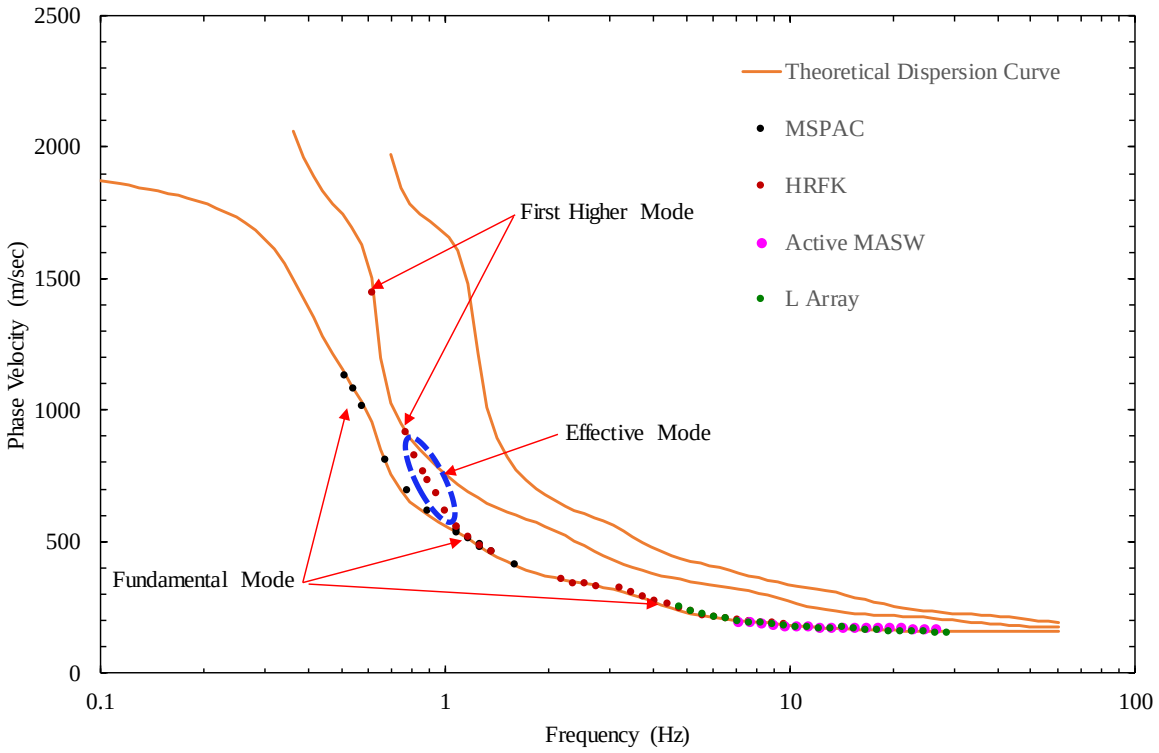

Figure 14. An example higher mode and effective mode data identification process is shown for Rayleigh wave dispersion data. The minimum misfit theoretical dispersion curve is shown along with the experimental data produced from active MASW, passive circular HRFK and MSPAC, and L-array. The HRFK data demonstrate a transition around 1 Hz and shift from the fundamental towards the higher mode.

For each site, between one and two million inversion models were generated during the final inversion to insure the solution space was properly explored. For the misfit calculations, a weighting factors of 0.8 and 0.2 were used for the dispersion and HVSR data, respectively. A representative sample of the 1000 lowest misfit profiles are used to calculate the median Vs profile for the site. This provides a more rigorous Vs profile than the lowest misfit profile as the top 1000 lowest misfit profiles generally have very similar misfit values, meaning each provides a reasonable solution to the inversion problem (Teague *et al.*, 2015, Teague *et al.*, 2016, Deschenes *et al*., 2018).

Invasive

The shallow and deep downhole datasets collected at CUSSO were analyzed to develop shear wave velocity profiles at the site. The shallow downhole dataset was analyzed using the corrected vertical travel time versus depth analysis method (Redpath 2007, Wood 2009). The raw signals recorded in the field were digitally filtered with a zero phase shift low pass filter at 400 Hz for P-waves and 200 Hz for shear waves. The horizontal components of the downhole tool were rotated to the highest amplitude azimuth to orient one horizontal component in-line with the E-W oriented shear beam. The P-waves and S-waves were then plotted in a waterfall plot and the first peak for the P-wave was picked and first peak/trough was picked for the S-waves. This time was corrected for onset since the first arrive was not picked and corrected for the offset of the source from the borehole. The velocities and depths to different layers are then identified from the vertical travel time vs depth plot of the P-wave and S-wave arrival times.

The deep downhole dataset was also analyzed using the corrected vertical travel time versus depth analysis method (Redpath 2007, Wood 2009). The horizontal components of the downhole tool were first rotated to the highest amplitude azimuth to orient one horizontal component in-line with the cross-line vibroseis signal. The raw signals recorded in the field were cross correlated with the true reference source signal for each depth and the highest amplitude of the cross correlation was chosen as the travel time at each depth. This time was corrected for the offset of the source from the borehole. The velocities and depths to different layers are then identified from the vertical travel time vs depth plot of the S-wave arrival times.

Results and Discussion

In this chapter, the results of the dynamic site characterization measurements at each site are discussed individually. The results include: (1) the experimental dispersion data measured in the field along with the theoretical dispersion curves computed from the generated shear wave velocity profiles, (2) comparison of experimental HVSR curves and theoretical ellipticity curves generated from the shear wave velocity profiles, (3) shear wave velocity profile from the inversion along with the CUSVM geological layers.

Finally, a table summarizing the average V_S in top 30 m (V_{S30}), median formation depth of Memphis sand, and median formation velocity of Memphis sand at each site are provided.

(i) **CUSSO:** The CUSSO site is situated in Fulton County, Kentucky. This site is geologically located in the lowland part of the Mississippi Embayment with Holocene age-deposits at the

surface and a bedrock depth of 585 m (Woolery *et al.*, 2016). This site has three boreholes equipped with a vertical seismic array; the deepest one is 587 meter extending down to the Paleozoic bedrock. At this site, surface wave data were collected using a 46 m linear active MASW array, a 60x55 m L-array, and circular arrays of diameter 50 m, 200 m, and 500 m. Downhole measurements were also made at the 259 m borehole and 587 m borehole.

The experimental Rayleigh and Love dispersion data for the CUSSO site are shown in Figure 15 (a) and (b), respectively. For the Rayleigh wave dispersion data, the active MASW dispersion data ranged from approximately 7 – 30 Hz, overlapping the L-Array data in this entire range. The L-array dispersion data reached a low frequency of approximately 3 Hz, overlapping with the HRFK dispersion data. The scattered MSPAC data ranged from 0.3 – 3.5 Hz, and have a similar trend with the HRFK dispersion data. The HRFK dispersion data reached the lowest frequency compared with the other methods (approximately 0.25 Hz). The Love wave active MASW dispersion data covered a range of 7 – 45 Hz with an overlapping zone with the Love HRFK dispersion data. The Love HRFK dispersion data reached a low frequency of 1 Hz.

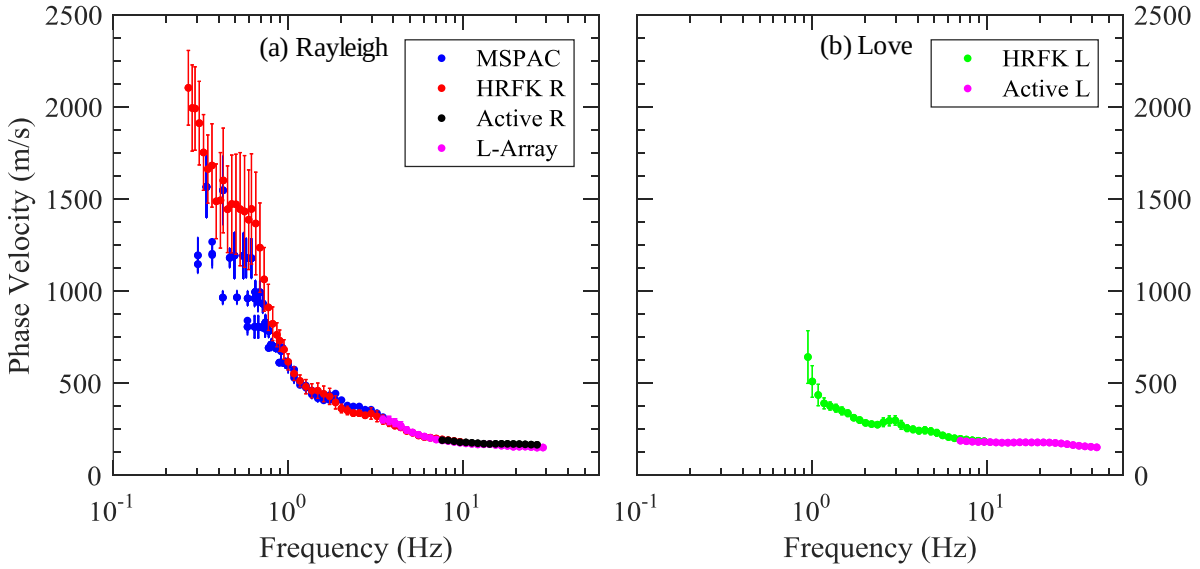

Figure 15. Composite experimental dispersion data shown for the CUSSO site, (a) Rayleigh and (b) Love.

In Figure 16, the theoretical dispersion curve and ellipticity results for the CUSSO SWM are shown. The experimental dispersion data and the 1000 lowest misfit theoretical curves along with their counted median dispersion curve is shown for Rayleigh and Love waves in Figure 16 (a) and (b), respectively. As discussed in the data processing section, all the effective mode data were removed and the proper mode was assigned to each dispersion point. The minimum misfit between the theoretical and experimental data was 0.54.

The median of the 1000 best SWM V_S profiles was used to compute the theoretical fundamental mode Rayleigh wave ellipticity as shown in Figure 16 (c). The theoretical ellipticity peak, $f_{0,thr}$ was determined to be 0.297 Hz, which is within one standard deviation of the experimental HVSR peak of 0.292 Hz.

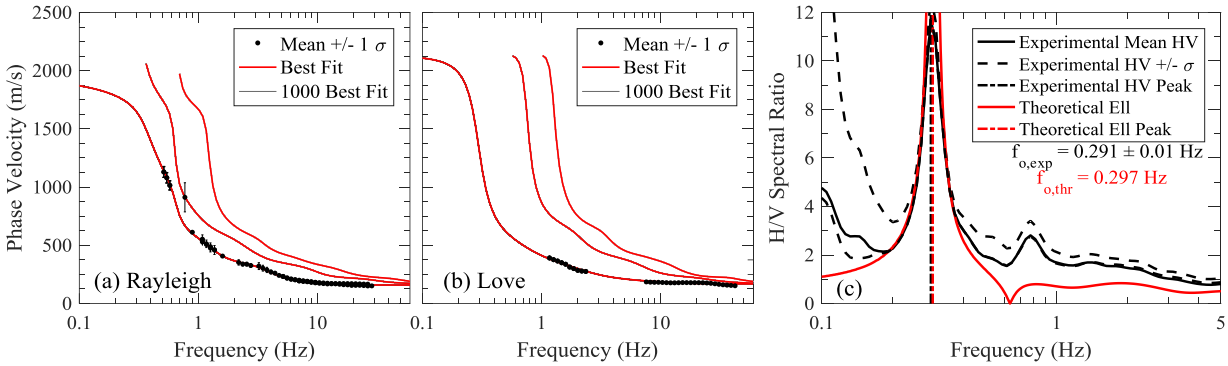

Figure 16. Experimental dispersion data and theoretical fits for the 1000 lowest misfit V_S profiles at CUSSO site are shown for (a) Rayleigh wave and (b) Love wave, respectively. The experimental HVSR curve and the theoretical ellipticity curve associated with the median V_S profile are shown in (c).

A plot of the corrected P- and S-wave vertical travel time versus depth for the shallow downhole measurements in the 259 m borehole at CUSSO, together with the corresponding interpreted values of velocity and depths to layer interfaces are shown in Figure 17. The P-wave velocities observed in the borehole in the top 5 m indicated reasonable velocities for the soil layers of 360 m/s. However, below 5 meters, the velocity of the P-waves was 3100 m/s, which is near the P-wave velocity of steel indicating that the P-waves generated at the surface likely traveled down the steel casing instead of through the soil structure making the observed P-wave velocities unusable. Despite the poor results from the P-waves, good velocities were observed for the S-waves in the 259 m borehole. A 5 m thick layer with a velocity of 160 m/s is observed at the surface followed by a 235 m/s layer extending to 21 m. This layer is followed by a 280 m/s layer that extends to 37 m. The final layer in the Vs profile has a Vs of 385 m/s and extends to at least 115 m (the full depth of the profile).

A plot of corrected S-wave vertical travel time versus depth for the deep downhole measurements in the 587 m borehole at CUSSO, together with the corresponding interpreted values of velocity and depths to layer interfaces are shown in Figure 18. A number of layers were observed in the top 50 meters of the borehole, but the velocities in these layers are considered less reliable than the shallow downhole results due to the coarse measurement spacing, therefore the results are not shown in the figure. Below 50 meters, a similar velocity of 385 m/s was observed and extends to 125 m. At 125 m, a major velocity increase to 600 m/s is observed which extends down to 205 m. The velocity contrast corresponds with the lower middle Claiborne or Memphis sand formation. Below 205 m, two stiffer layers are observed with Vs of 675 m/s and 700 m/s and extend to 255 m and 390 m, respectively. At 390 m, a softer layer is observed with a velocity of 620 m/s. This layer corresponds with the Porters Creek clay or Paleocene formation. This layer extends to the final depth of the profile of 425 meters. To complete the downhole Vs profile to bedrock, the P-S suspension logger Vs from Woolery *et al.*, 2015 is used to include the Cretaceous layer with a Vs of 875 m/s starting at 495 m and extending down to bedrock at 585 m. A bedrock Vs of 2500 m/s was assumed for the profile based on the surface wave testing results discussed later in the report.

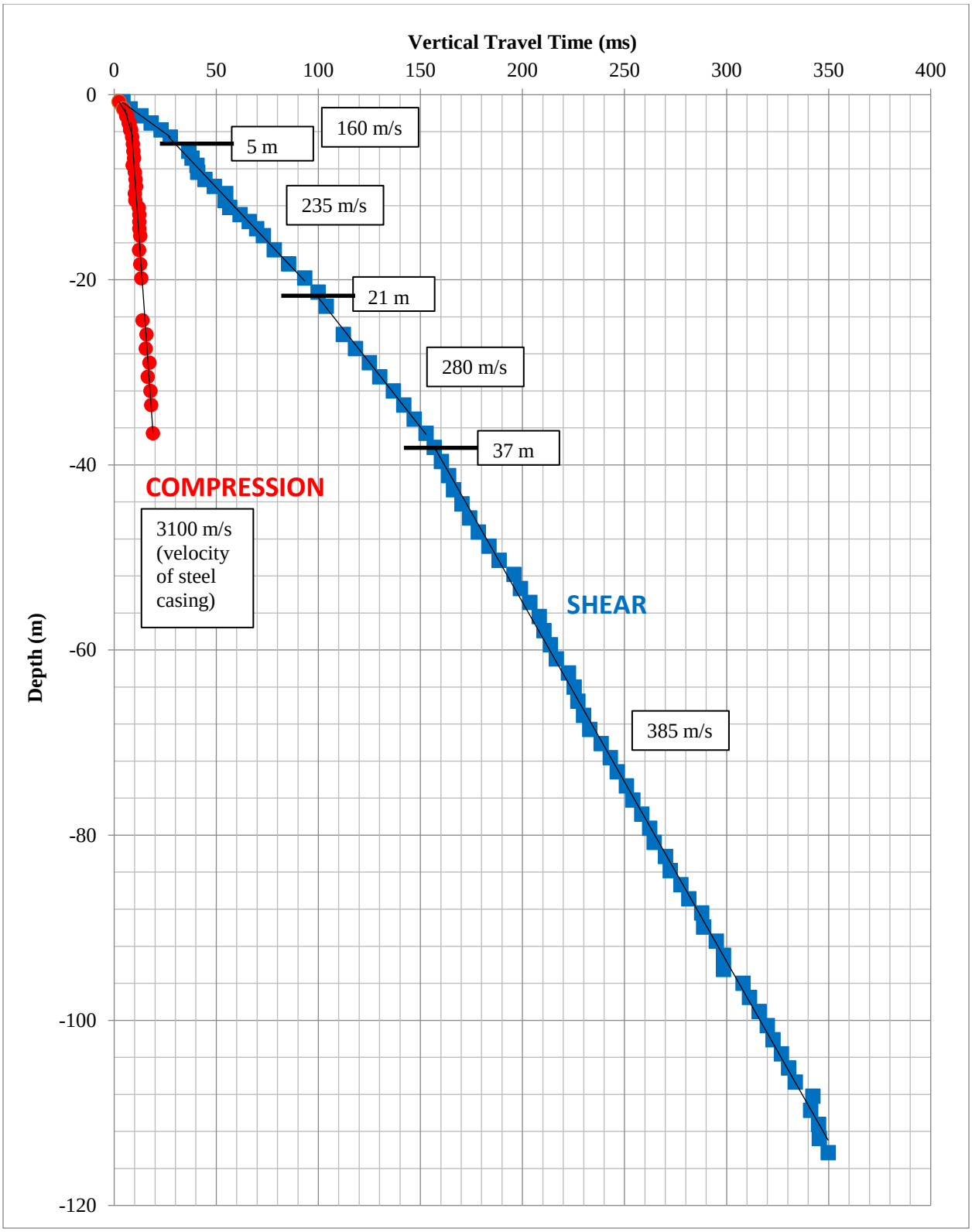

Figure 17. Vertical travel time versus depth plot for P- and S-wave arrivals obtained in the CUSSO 259 m borehole.

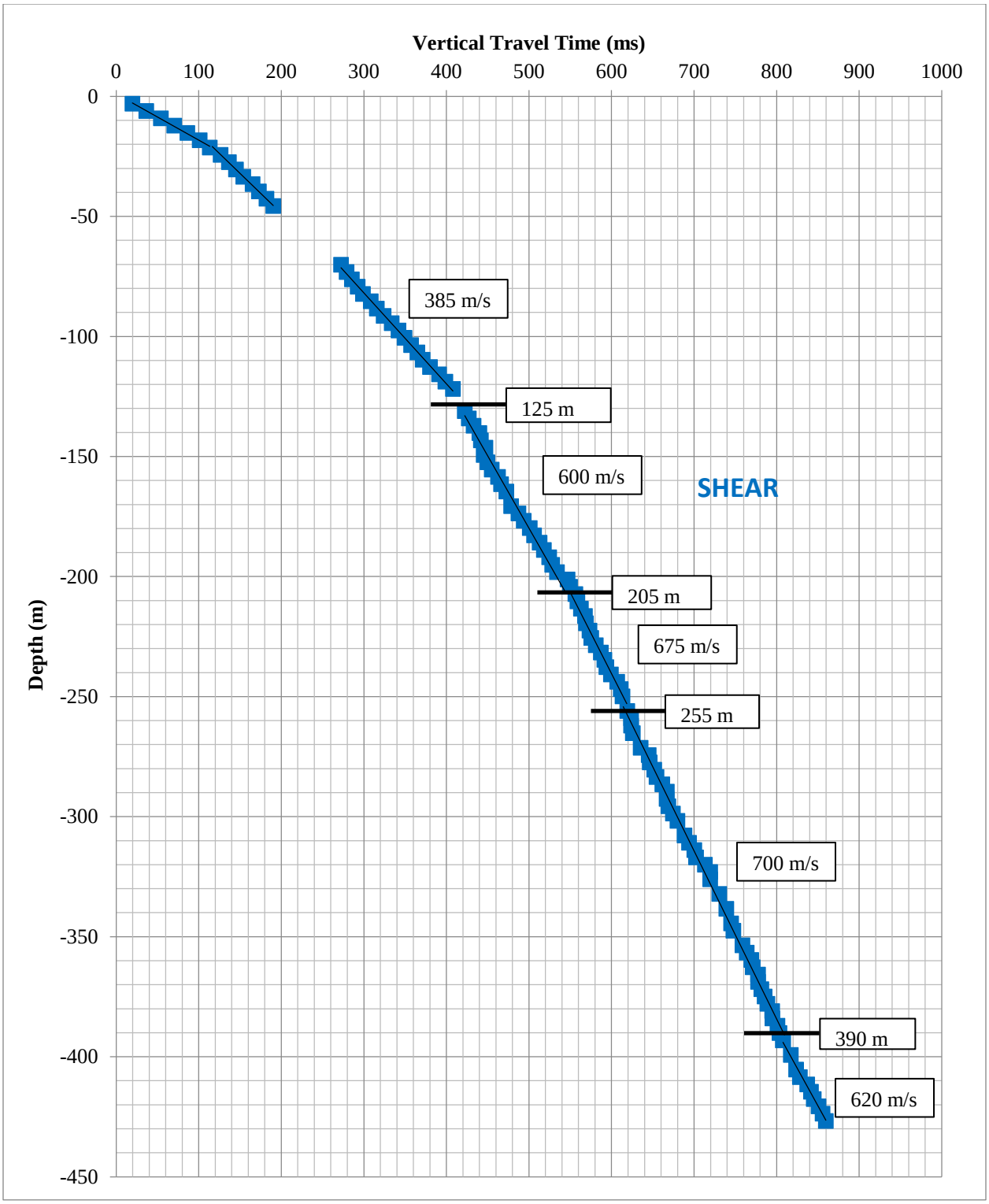

Figure 18. Vertical travel time versus depth plot for S-wave arrivals obtained in the CUSSO 587 m borehole.

In Figure 19, the SWM and downhole V_S profile results are shown. The 1000 lowest misfit models, the counted median V_S, the 5^{th} and 95^{th} percentile confidence intervals of V_S from the 1000 lowest misfit V_S profiles, and the standard deviation of natural logarithm of the V_S magnitudes ($\sigma \ln(Vs)$) are presented for (a) the first 200 m and (b) to 1000 m deep. In addition, Woolery *et al.*, 2016, Ramirez-Guzman *et al.*, 2012 (CUSVM), and Romero and Rix, 2005 lowland are shown for comparison. Reference V_S profiles from Lin *et al.*, 2014 for several materials are added. Geologic unit boundaries from CUSVM are shown for the CUSSO site with different color codes for each geologic unit.

The downhole, and SWM V_S profiles are consistent throughout much of the profile. From 45 m to approximately 70 m depth, both profiles have velocity ranges between dense sand and dense gravel, which is consistent for the stiff clay and sand formation layers found in the Upper Tertiary. From 90 m down to approximately 120 m these profiles became softer than the dense sand, but at 120 – 130 m, both profiles have a increase in velocity, which indicates the Lower Middle Claiborne or Memphis sand layer. However, for the Woolery *et al.*, 2016 Vs profile, the Memphis sand depth is around 85 m, which is close to the Memphis sand depth of CUSVM. The downhole measurement V_S profile resolves the Memphis sand depth at 125 m, which is coherent with surface wave profiles resolving the layer at 130 m. The Woolery *et al.*, 2016 V_S profile shows another increase in velocity within the Jackson formation, which is not observed in any other V_S profiles. After reaching the Memphis sand depth, all the V_S profiles demonstrate a higher velocity within the dense sand and dense gravel reference velocity down to 200 m. The CUSVM profile is at most depths softer than any other V_S profiles down to 200 m and does not show a distinct increase around the Memphis sand impedance contrast. Within the Paleocene layer, the downhole V_S profile becomes stiffer than all the other V_S profiles down to 390 m. At 390 m depth, the downhole profile encounters a 105 m thick velocity inversion layer, which the SWM profile or the Woolery *et al.*, 2016 profile could not resolve. Lack of resolution could be one of the reasons that the SWM profile could not resolve the soft layer situated in the Paleocene unit. All V_S profiles except the CUSVM and Romero and Rix, 2005 lowland showed the start of Upper Cretaceous layer to be around 490 m with velocity of 850 – 900 m/sec, which is consistent with soft rock. The CUSVM Upper Cretaceous layer starts from 517 m. The Paleozoic bedrock layer depth for the surface wave inversion method was fixed at 585 m, the same as the Woolery *et al.*, 2016, whereas the CUSVM shows the Paleozoic layer to be at 604 m. All the V_S profiles other than the Woolery *et al.*, 2016 have a bedrock V_S ranging from 2130 – 2500 m/sec, whereas the Woolery et al., 2016 profile has a 1452 m/sec bedrock V_S.

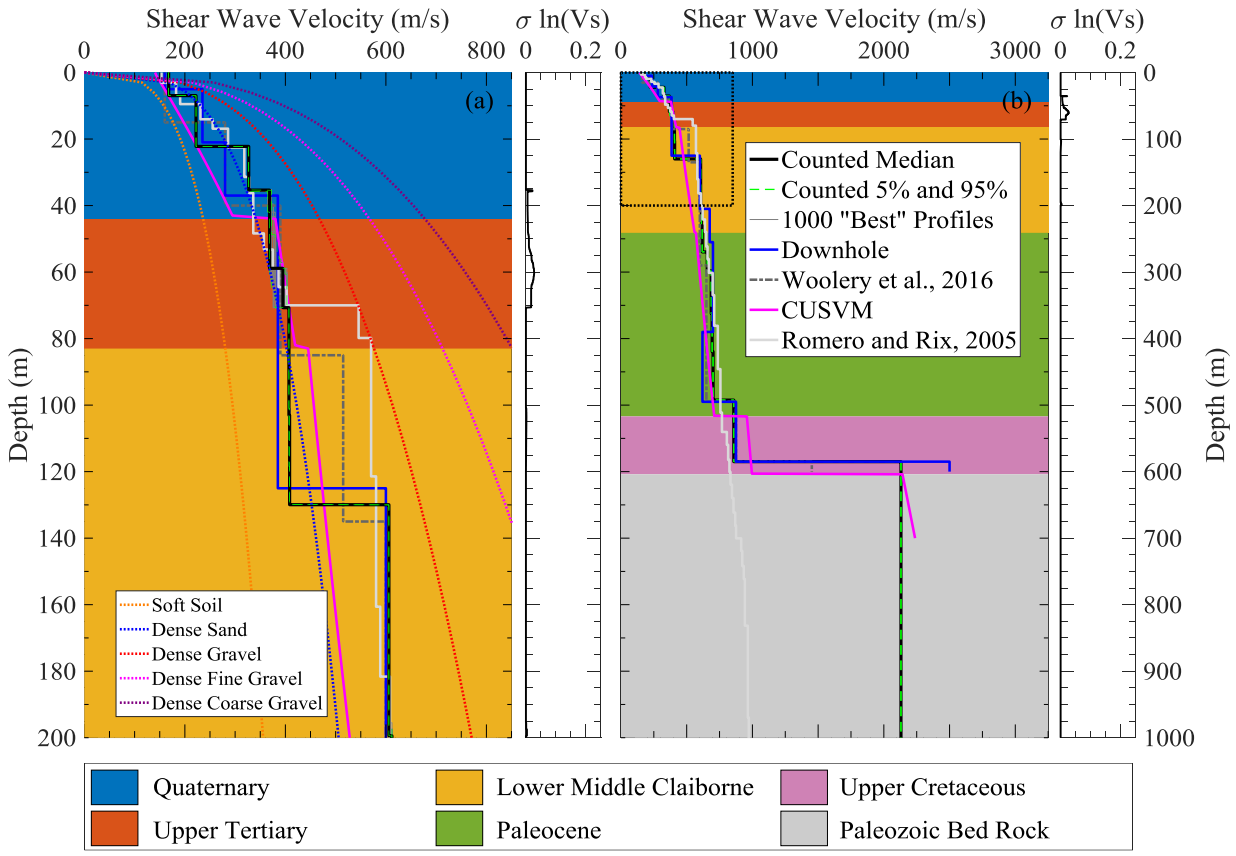

Figure 19. Shear wave velocity profiles resulting from inversion for the CUSSO site are shown. One thousand best V_S profiles along with their counted median for the CUSSO are shown. The V_S profiles from CUSSO downhole measurements, Woolery *et al.*, 2016, Ramirez-Guzman *et al.*, 2012 (CUSVM) and Romero and Rix, 2005 lowland profiles are also included for comparison. The σln(Vs) is for the CUSSO profiles demonstrating the uncertainty in the V_S. The blue dashed lines represent the counted 5th and 95th percentile V_S confidence interval for the 1000 CUSSO profiles. Reference V_S profiles from Lin *et al.*, 2014 for different soil types are also included. Geologic unit boundaries from CUSVM are shown for the CUSSO site with different color codes.

The theoretical Rayleigh wave fundamental mode ellipticity peaks and shear wave transfer function peaks were calculated for all the V_S profiles at the CUSSO site and shown in the Table 2. The V_S profiles developed using the SWM were consistent with the downhole measurements. The time averaged V_S to bedrock for the downhole, and median of SWM Vs profiles are 553.2 m/sec, and 557.5 m/sec, respectively. The percent difference between the SWM average V_S and the downhole average V_S is less than 1.0%. Based on the averaged V_S, ellipticity peaks, and transfer function peaks, the SWM inversion V_S profiles are in good agreement with the downhole V_S profile and the fundamental period of the site. These facts also corroborate the validation of the SWM to develop the deep shear wave velocity for the rest of the sites.

Table 2. Theoretical fundamental Rayleigh wave ellipticity peaks, shear wave transfer function peaks and their percent difference with the experimental HVSR peak are shown. Here, in the percent difference, a '+' sign refers to higher value than the HVSR peak and vice versa.

V_S Profile	Ellipticity Peak (Hz)	% difference from Exp. HVSR peak	Transfer Function Peak (Hz)	% difference from Exp. HVSR peak
SWM Median profile	0.297	+1.9	0.310	+6.3
Downhole	0.282	-3.2	0.300	+2.6
Woolery et al., 2016	0.404	+38.6	0.305	+4.6
CUSVM	0.278	-4.6	0.287	-1.5
Romero and Rix, 2005	0.253	-13.2	0.2215	-24.0

(ii) **TUMT:** The TUMT site is situated inside the University of Memphis campus. Geologically this site is located in the highland part of the Mississippi Embayment with Pleistocene age deposits at the surface and has a bedrock depth of 923 m (Ramirez-Guzman *et al.*, 2012). The seismic station at this site is situated near the Center for Earthquake Research and Information (CERI) building. Due to space constraints near the station, surface wave testing was conducted in two areas-one near the station, with a smaller circular array and the other one in the adjacent field (140 m away) using larger circular arrays; the associated data and results from the former and later are termed as TUMT station and TUMT, respectively. For TUMT station, a 46 m long active MASW array, a 60x55 m L-array, and a circular array of approximately 50 m diameter were used to record the surface wave data. For TUMT, surface wave data were collected using a 46 m linear active MASW array, a 60x55 m L-array, and circular arrays of diameter 50 m, 200 m, and 500 m.

The experimental dispersion data for the Rayleigh and Love wave data collected at TUMT are shown in Figure 20 (a) and (b), respectively. The Rayleigh wave MASW data ranged from approximately 9 – 44 Hz, overlapping with some parts of the L-Array dispersion data. The L-Array dispersion data resolved as fundamental mode at higher frequency, but jumps to a unidentified effective/higher mode below 13 Hz. The scattered MSPAC data overlapped with the HRFK data from 1 – 3 Hz and were able to reach down to approximately 0.4 Hz. However, there is a separation between the MSPAC and HRFK data at less than 1 Hz, indicating higher or effective mode behavior. The MASW Love data has a similar trend as the HRFK Love data and covers a range from 7 – 44 Hz. The Love HRFK data extend down to 1 Hz at 670 m/sec.

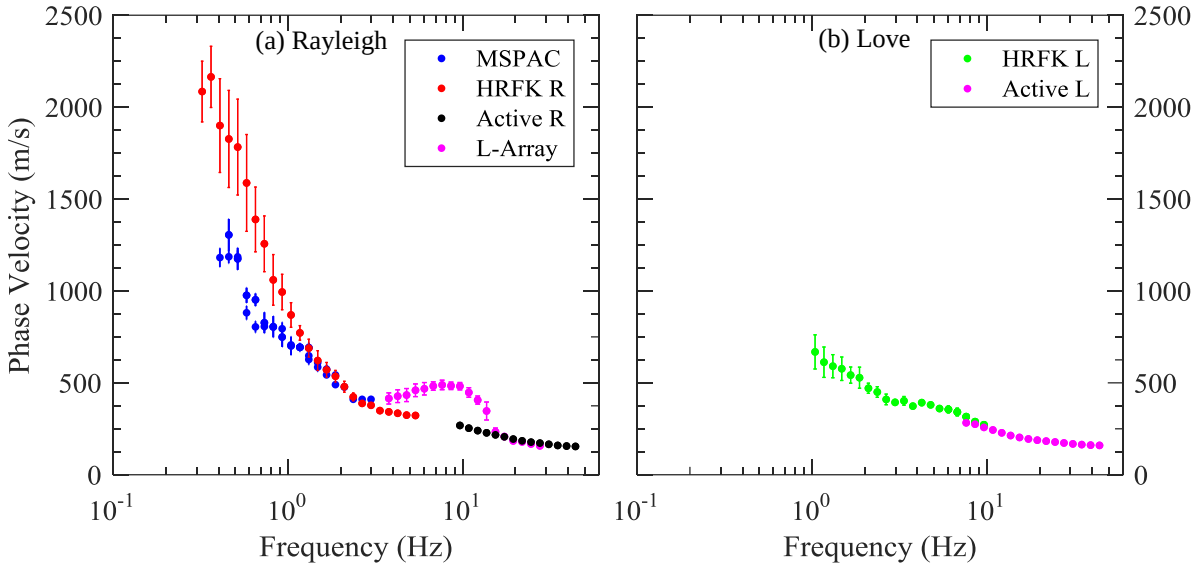

Figure 20. Composite experimental dispersion data shown for the TUMT site, (a) Rayleigh and (b) Love.

The surface wave data recorded at TUMT station are shown in the Figure 21 (a) and (b), respectively for Rayleigh and Love wave. The active MASW data from this area seems to have some effective/higher mode as it does not follow the trend of L-Array or the HRFK data. The L-Array data were able to fit the trend with the HRFK data and covered a range of 3 – 27 Hz. Due to the smaller sized circular array, the HRFK or the MSPAC data could not reach lower than 1.5 Hz at 560 m/sec. Thus, the depth of exploration from this surface wave data is expected to not go beyond 200 m. The Love wave active MASW and HRFK have similar trends and cover a range of frequencies from 3 – 40 Hz.

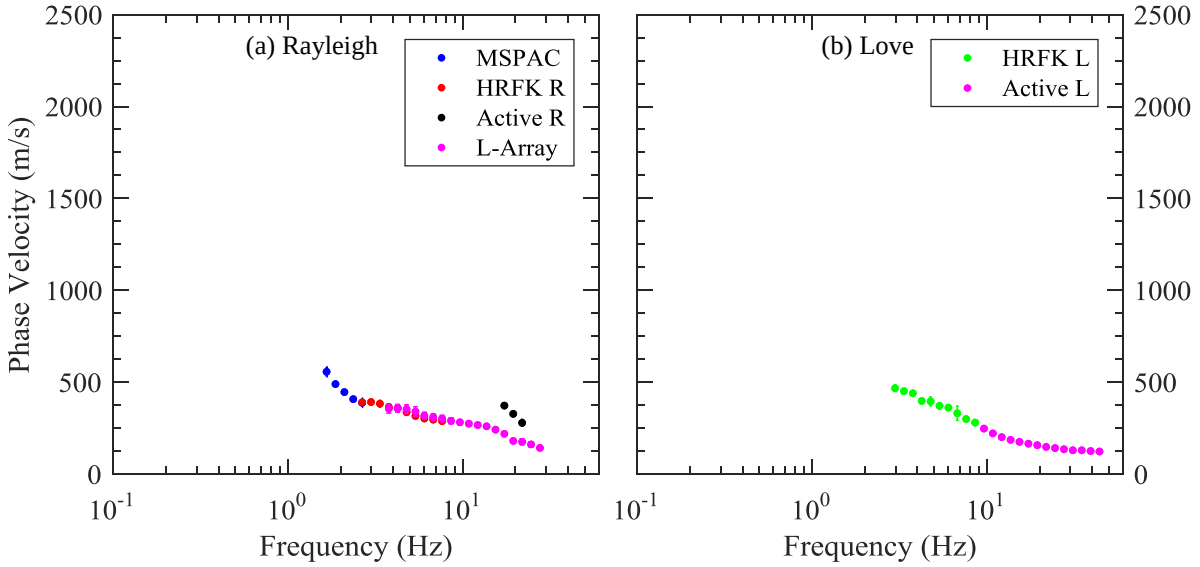

Figure 21. Composite experimental dispersion data shown for the TUMT station, (a) Rayleigh and (b) Love.

In Figure 22 (a) and (b), the experimental dispersion data and the 1000 lowest misfit theoretical curves along with their counted median dispersion curve are shown for Rayleigh and Love wave, respectively. All effective mode data and the outlier data points were removed through iterations and proper modes were assigned to the rest of the data. The minimum misfit for the TUMT data was 0.20. The median of the 1000 best TUMT V_S profiles was used to compute the theoretical fundamental mode Rayleigh wave ellipticity as shown in Figure 22 (c). The theoretical ellipticity peak, $f_{0,thr}$ was determined to be 0.22 Hz, which is within one standard deviation of the experimental HVSR peak of 0.225 Hz.

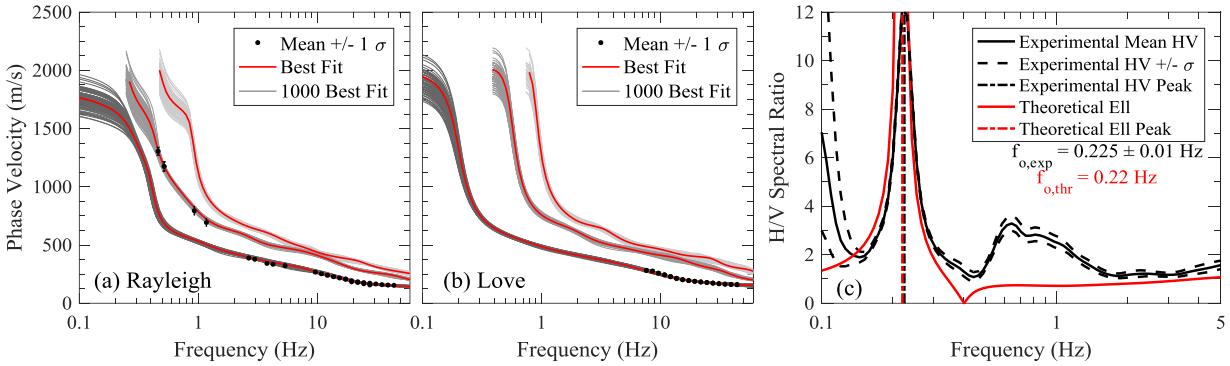

Figure 22. Experimental dispersion data and theoretical fits for the 1000 lowest misfit V_S profiles at TUMT are shown for (a) Rayleigh wave and (b) Love wave, respectively. The experimental HVSR curve and the theoretical ellipticity curve associated with the median V_S profile are shown in (c).

The experimental dispersion data along with their theoretical fit from the 1000 best profiles for TUMT station data are shown in Figure 23 (a) and (b) for Rayleigh and Love, respectively. As the largest circular array for this site was approximately 50 m in diameter, the lowest surface wave data to fit the theoretical curve was around 3.0 Hz. The HVSR fundamental peak, which is 0.225 Hz was not used during the joint inversion to constrain the bedrock depth, as it was lower than the lowest recorded surface wave data from this area. Thus, to resolve the V_S profile down to the shallow impedance contrast from Memphis sand, the second HVSR peak around 0.65 Hz was used along with the surface wave data for joint inversion. A Memphis sand depth range of 150 – 200 m was used in the parameterization to resolve this layer.

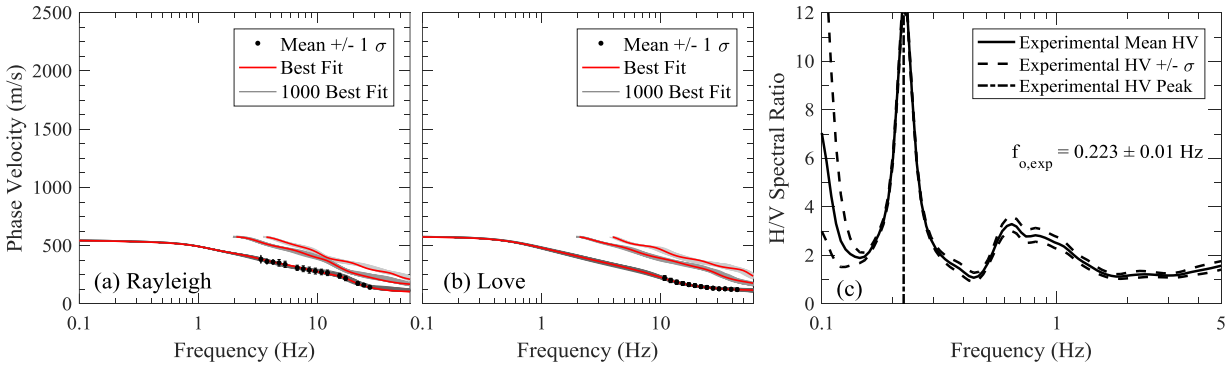

Figure 23. Experimental dispersion data and theoretical fits for the 1000 lowest misfit V_S profiles at the TUMT station are shown for (a) Rayleigh wave and (b) Love wave, respectively. The experimental HVSR curve is shown in (c).

The V_S results from the TUMT and TUMT station inversion are shown in Figure 24. For TUMT, the 1000 best V_S profiles along with their counted median are shown, but for the TUMT station, only the counted median from its 1000 best V_S profiles is shown. In addition, the V_S profiles from Ramirez-Guzman *et al.*, 2012 (CUSVM), and Romero and Rix, 2005 highland are shown for comparison. Reference V_S profiles from Lin et al., 2014 for several materials are added.

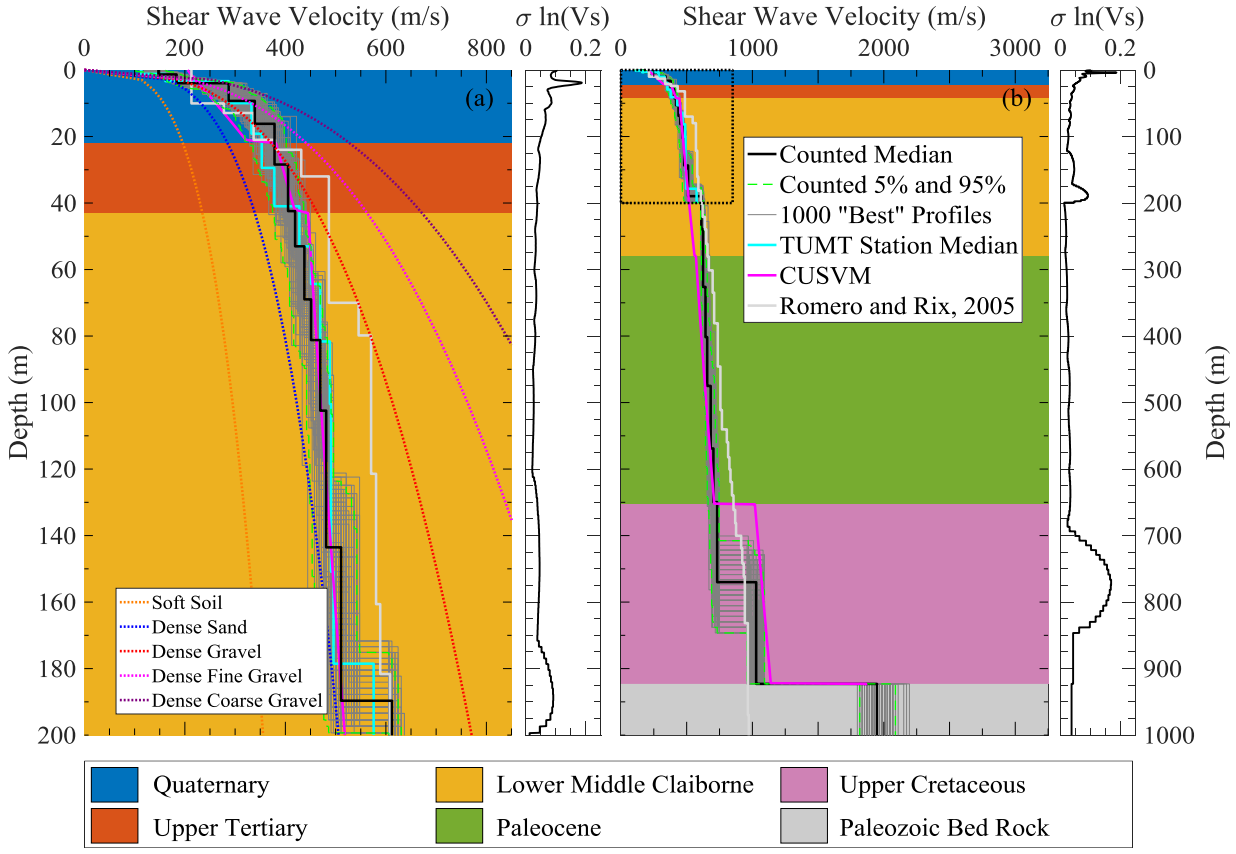

Figure 24. One thousand best V_S profiles along with their counted median for TUMT are shown, whereas only the median V_S profile from the TUMT station is shown for easy comparison with the other V_S profiles. V_S profiles from Ramirez-Guzman *et al.*, 2012 (CUSVM) and Romero and Rix, 2005 highland are also included for comparison. The σln(Vs) is for the TUMT profiles demonstrating the uncertainty in the V_S. The blue dashed lines represent the counted 5th and 95th percentile V_S confidence interval for the 1000 TUMT profiles. Reference V_S profiles from Lin *et al.*, 2014 for different soil types are also included. Geologic unit boundaries from CUSVM are shown for TUMT with different color codes.

From the Vs profiles in Figure 24a, both TUMT and TUMT station V_S profiles are consistent down to 180 m. The CUSVM V_S profile is softer in the Quaternary layer, but later becomes consistent with the SWM results down to 190 m. The Romero and Rix, 2005 highland V_S profile is stiffer than all profiles from 30 m down to approximately 180 m. All V_S profiles except the Romero and Rix, 2005 highland are within the dense sand and dense gravel reference V_S in the Upper Tertiary layers, which is consistent with the stiff clay and sand formation found in the Upper Tertiary. The CUSVM projected Memphis sand depth at this site is around 45 m, but the both SWM V_S profiles show the Memphis sand layer starting around 150 – 190 m. The TUMT

station median V_S indicates the Memphis sand interface is around 180 m, whereas the TUMT median V_S profile resolves the layer around 190 m. This difference may be due to the elevation difference between these two sites, which is approximately 8 m. The CUSVM profile did not show any distinct increase of V_S at the Memphis sand interface. The SWM results have V_S ranging of 580 – 612 m/sec for the Memphis sand, which is consistent with Rosenblad *et al.*, 2010. The CUSVM profile is softer than the other Vs profiles below 200 m, but is consistent with the SWM results from approximately 300 m until the Upper Cretaceous layer. The SWM resolved the Upper Cretaceous layer at a depth ranging from 700 – 850 m, whereas the CUSVM profile indicates the layer should start around 650 m. The Paleozoic bedrock V_S ranged from 1800 – 2200 m/sec, which is consistent with the CUSVM bedrock velocity around 1850 m/sec.

(iii) **LNXT:** The LNXT seismic station is situated in Dyer County, Tennessee, near the Tennessee-Missouri border. Geologically this site is located in the highland part of the Mississippi Embayment nearby the highland-lowland boundary line (Figure 3). The surface deposits at this site are Pleistocene age and the site has a bedrock depth of 845 m ((Ramirez-Guzman *et al.*, 2012). Due to space constraints near the seismic station, the regular sized L-Array could not be used at this site. Thus, a 68x24 m L-array with 4 m receiver spacing was used instead of a 60x55 m L-Array. All other regular arrays, such as the 46 m long active MASW, and circular arrays of 50 m, 200 m, and 500 m were used for recording the surface wave data.

The experimental dispersion data for the Rayleigh and Love wave data collected at the LNXT site are shown in Figure 25 (a) and (b), respectively. The Rayleigh active MASW data covered a frequency range of 9.5 – 45 Hz and fit well with the L-Array data. The L-Array and MSPAC, both had similar trends with the HRFK Rayleigh data. MSPAC data overlapped with the HRFK Rayleigh data from 0.8 – 2.5 Hz. The lowest frequency reached was by the HRFK Rayleigh at 0.25 Hz with a phase velocity of 2050 m/sec. The Love active MASW data had a similar trend to the Love HRFK data and cover a frequency range of 7.5 – 45 Hz with overlapping segments with the HRFK Love. The HRFK Love data reached down to 1 Hz with a phase velocity of 680 m/sec.

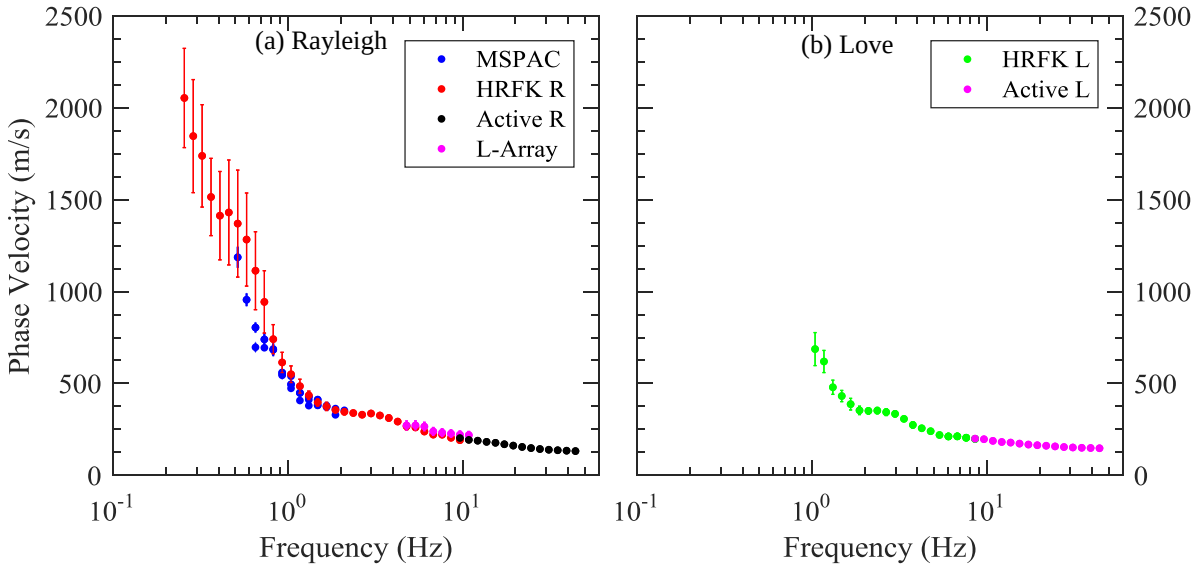

Figure 25. Composite experimental dispersion data shown for LNXT site, (a) Rayleigh and (b) Love.

In Figure 26 (a) and (b), the experimental dispersion data and the 1000 lowest misfit theoretical curve along with their counted median dispersion curve are shown for Rayleigh and Love waves, respectively. After rigorous iterative processing to remove the effective mode data and assigning the proper modes to the rest of the data, the final model had a minimum misfit of 0.27 between the experimental data and theoretical fit. The median of the 1000 best LNXT site V_S profiles was used to compute the theoretical fundamental mode Rayleigh wave ellipticity as shown in Figure 26 (c). The theoretical ellipticity peak, $f_{0,thr}$ was determined to be 0.242 Hz, which is within one standard deviation of the experimental HVSR peak of 0.245 Hz.

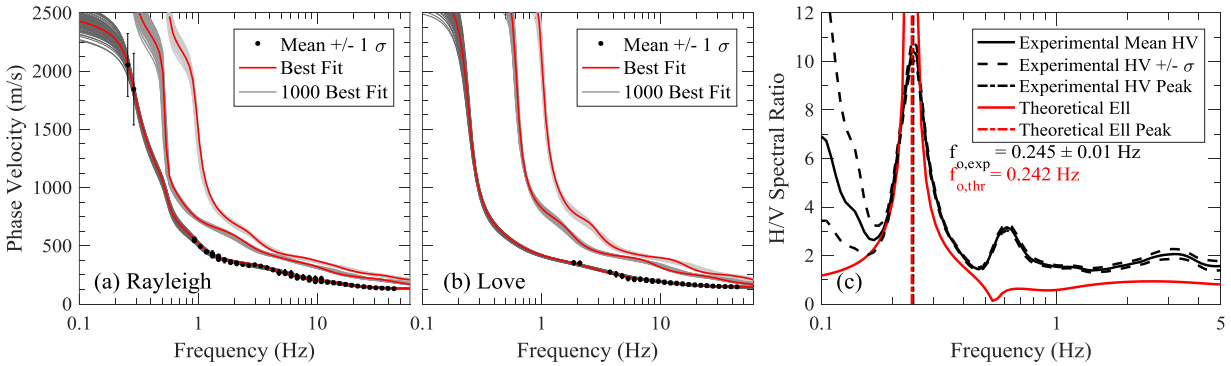

Figure 26. Experimental dispersion data and theoretical fits for the 1000 lowest misfit V_S profiles at the LNXT are shown for (a) Rayleigh wave and (b) Love wave, respectively. The experimental HVSR curve and the theoretical ellipticity curve associated with the median V_S profile are shown in (c).

The V_S results from the LNXT inversions are shown in Figure 27. The one thousand best V_S profiles along with their counted median are shown. In addition, the V_S profiles from Ramirez-Guzman *et al.*, 2012 (CUSVM), and Romero and Rix, 2005 highland V_S profiles are shown for comparison. Reference V_S profiles from Lin et al., 2014 for several materials are added.

For the Vs profile in Figure 27a, the Romero and Rix, 2005 highland V_S profile is stiffer than the SWM Vs profile from approximately 10 m down to 170 m, whereas the CUSVM V_S profile is softer down to approximately 60 m. The Romero and Rix, 2005 highland V_S profile has an increase in Vs at the Quaternary-Upper Tertiary interface, which is absent in the CUSVM and SWM V_S profiles. This makes the Romero and Rix, 2005 highland about 25% stiffer than the SWM and CUSVM V_S profiles at this site in the Upper Tertiary layer. The CUSVM V_S profile at the LNXT has a more consistent Memphis sand depth with the SWM result at this site than the previously discussed sites. However, the velocity increase at the Memphis sand depth in the CUSVM V_S profile is about 30 m/sec, reaching a V_S of 445 m/sec, whereas the median SWM V_S profile has a V_S around 600 m/sec at a depth of 170 m. The Romero and Rix, 2005 highland V_S profile is consistent with the SWM profile from approximately 200 m down to 690, whereas the CUSVM is softer in this whole depth range. At LNXT, the Cretaceous layer is resolved in both the CUSVM and SWM V_S profile at similar depth around 700 m. The bedrock V_S ranges from 2500 – 2900 m/sec for the SWM, whereas the CUSVM demonstrates a bedrock V_S of 2350 m/sec.

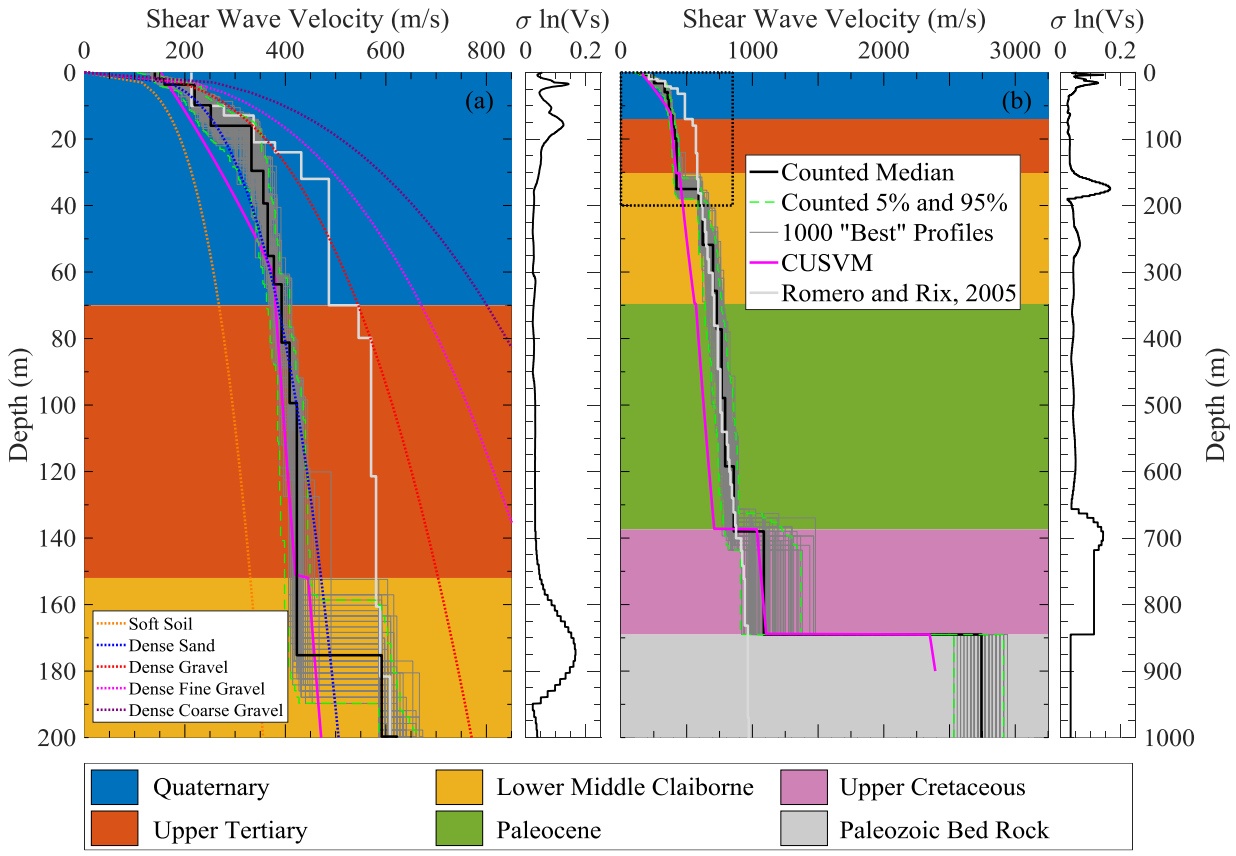

Figure 27. One thousand best V_S profiles along with their counted median for LNXT are shown. The V_S profiles from Ramirez-Guzman *et al.*, 2012 (CUSVM) and Romero and Rix, 2005 highland profiles are also included for comparison. The σln(Vs) is for the LNXT profiles demonstrating the uncertainty in the V_S. The blue dashed lines represent the counted 5th and 95th percentile V_S confidence interval for the 1000 LNXT profiles. Reference V_S profiles from Lin *et al.*, 2014 for different soil types are also included. Geologic unit boundaries from CUSVM are shown for LNXT with different color codes.

(iv) **HBAR:** The HBAR seismic station site is situated in Poinsett County, Arkansas. Geologically this site is located in the lowland part of the Mississippi Embayment. The surface deposits at this site are Holocene age and the site has a bedrock depth of 754 m (Ramirez-Guzman *et al.*, 2012). At this site, surface wave data were collected using a 46 m linear active MASW array, a 60x55 m L-array, and circular arrays of diameter 50 m, 200 m, and 500 m.

The experimental dispersion data for the Rayleigh and Love wave data collected at the HBAR site are shown in Figure 28 (a) and (b), respectively. The Rayleigh active MASW data covers a frequency range of 6.5 – 45 Hz, and overlaps with the L-Array data around 7 Hz, showing no sign of near-field effects present in the active data. The L-Array data fill the gap between the active MASW and HRFK Rayleigh and overlaps with the HRFK Rayleigh and MSPAC data covering a range of 3 – 6.5 Hz. The scattered MSPAC data has a similar trend to the HRFK Rayleigh down to 1.5 Hz but later has lower phase velocity than the HRFK data, which is probable at low frequencies for MSPAC data (Asten and Boore, 2005). The lowest frequency reached by

HRFK Rayleigh is around 0.8 Hz with a phase velocity of 2000 m/sec. The Active Love MASW covers a frequency range of 7.5 – 45 Hz, and has a slightly higher phase velocity than the HRFK Love at their overlapping zone. The HRFK Love data reached down to 1.8 Hz with a phase velocity around 700 m/sec.

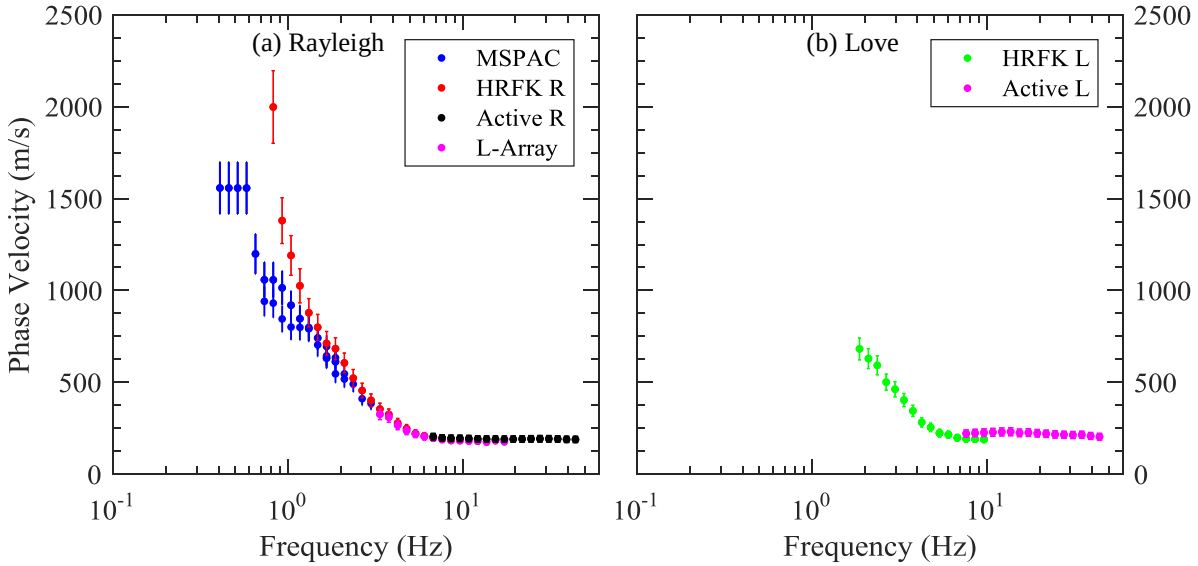

Figure 28. Composite experimental dispersion data shown for the HBAR site, (a) Rayleigh and (b) Love.

In Figure 29 (a) and (b), the experimental dispersion data and the 1000 lowest misfit theoretical curve along with their counted median dispersion curve are shown for Rayleigh and Love waves, respectively. The active MASW, L-Array, and HRFK Rayleigh data resolved fundamental mode dispersion data ranging from 3 – 45 Hz. MSPAC data were resolved as the first higher mode at 1.4 – 1.8 Hz and 0.65 – 0.75 Hz. All active Love MASW data ranging from 5 – 44 Hz were resolved as fundamental mode data. After numerous iterations to assign the correct modes to the experimental data and removing the effective mode data, the final 2 million model inversion had a minimum misfit of 0.25. The median of the 1000 best HBAR site V_S profiles was used to compute the theoretical fundamental mode Rayleigh wave ellipticity as shown in Figure 29 (c). The theoretical ellipticity peak, $f_{0,thr}$ was determined to be 0.253 Hz, which is within one standard deviation of the experimental HVSR peak of 0.252 Hz.

The V_S results from the HBAR site inversions are shown in Figure 30. The one thousand best V_S profiles along with their counted median are shown. In addition, the V_S profiles from Ramirez-Guzman *et al.*, 2012 (CUSVM), and Romero and Rix, 2005 lowland V_S profiles are shown for comparison. Reference V_S profiles from Lin et al., 2014 for several materials are added.

From the Vs profiles shown in the Figure 30a, a stiff increase in V_S in the CUSVM V_S profile is observed around 3 m, which is absent in the SWM and Romero and Rix, 2005 lowland V_S profile, making the CUSVM around 35 - 98% stiffer than the other two V_S profiles from 3 – 20 m. The SWM V_S profile resolved the likely Upper Tertiary layer at approximately 20 m deep, whereas the CUSVM V_S profile predicted it at a shallower depth of 3 m. All three V_S profiles have V_S values in between the dense sand and dense gravel reference Vs profiles in the Upper Tertiary layer, which is consistent with the stiff clay and sand formation in this layer. The CUSVM V_S profile

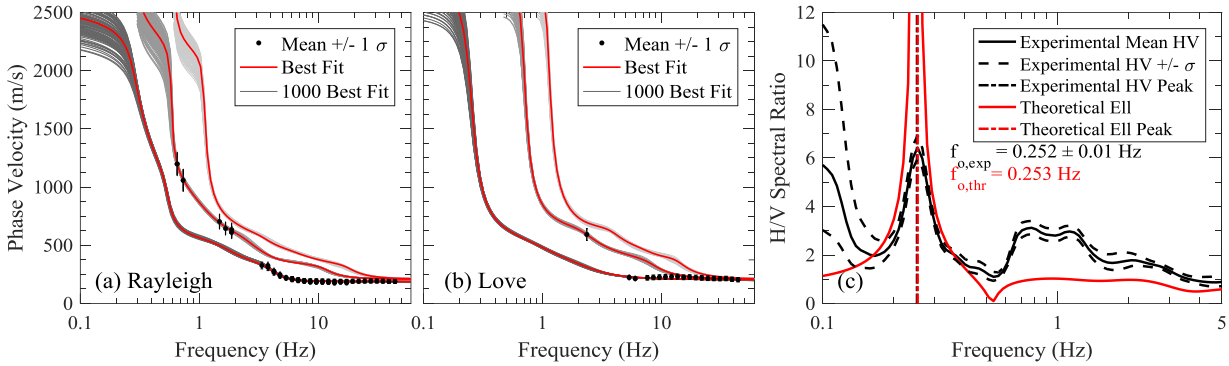

Figure 29. Experimental dispersion data and theoretical fits for the 1000 lowest misfit V_S profiles at the HBAR are shown for (a) Rayleigh wave and (b) Love wave, respectively. The experimental HVSR curve and the theoretical ellipticity curve associated with the median V_S profile are shown in (c).

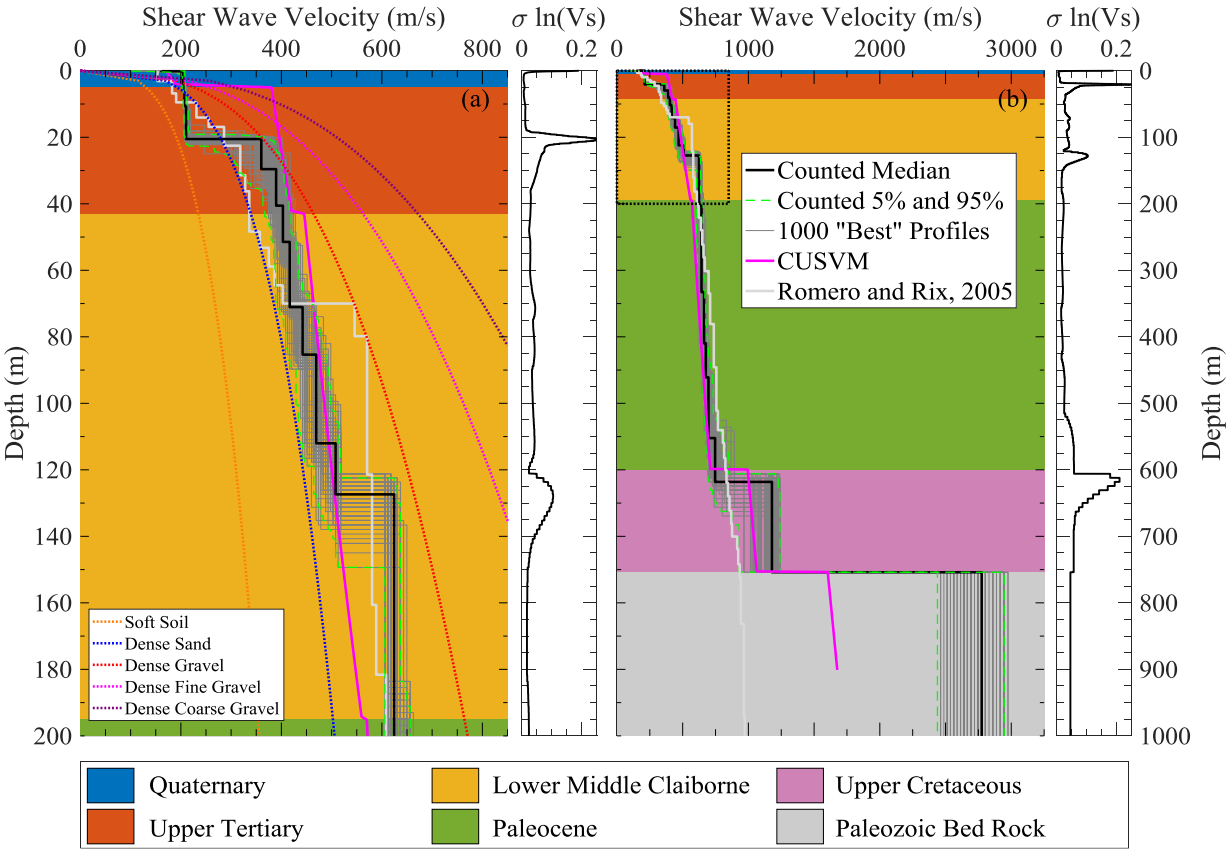

Figure 30. One thousand best V_S profiles along with their counted median for HBAR are shown. The V_S profiles from Ramirez-Guzman *et al.*, 2012 (CUSVM) and Romero and Rix, 2005 lowland profiles are also included for comparison. The σln(Vs) is for the HBAR profiles demonstrating the uncertainty in V_S. The blue dashed lines represent the counted 5th and 95th percentile V_S confidence interval for the 1000 HBAR profiles. Reference V_S profiles from Lin *et al.*, 2014 for different soil types are also included. Geologic unit boundaries from CUSVM are shown for HBAR with different color codes.

shows the start of Memphis sand layer at a depth at 45 m with a velocity of 445 m/sec. From the SWM V_S profile, the Memphis sand depth is resolved around 120 – 140 m with a shear wave velocity of 600 – 650 m/sec, which is consistent with Rosenblad *et al.*, 2010. The CUSVM and Romero and Rix, 2005 lowland V_S profiles are approximately 10 - 20% softer than the SWM V_S profile in the 120 – 300 m depth range. The Upper Cretaceous layer is resolved around 600 – 650 m deep in the SWM V_S profile, whereas the CUSVM V_S profile resolved the layer around 600 m. The bedrock V_S ranges from 2500 – 2900 m/sec for the SWM, whereas the CUSVM has a bedrock V_S of 1600 m/sec.

(v) **HENM:** The HENM seismic station site is situated in New Madrid County, Missouri. Geologically this site is located in the lowland part of the Mississippi Embayment. The surface deposits at this site are Holocene age and the site has a bedrock depth of 450 m (Ramirez-Guzman *et al.*, 2012). At this site, surface wave data were collected using a 46 m linear active MASW array, a 60x55 m L-array, and circular arrays of diameter 50 m, 200 m, and 500 m.

The experimental dispersion data for the Rayleigh and Love wave data collected at the HENM site are shown in Figure 31 (a) and (b), respectively. The Rayleigh active MASW covers a range of 6 – 45 Hz and overlaps with the L-Array data from 6 – 20 Hz, showing no sign of near-field effects. The L-Array data extends down to 3.2 Hz, and has a lower phase velocity than the HRFK Rayleigh at lower frequencies. The HRFK Rayleigh and MSPAC have similar trends down to 0.9 Hz. The MSPAC data has a lower phase velocity at frequencies less than 0.9 Hz compared to the HRFK, which is probable at the low frequency range (Asten and Boore, 2005). The HRFK Rayleigh's lowest frequency reached is 0.7 Hz with a phase velocity of 2050 m/sec. The Love active MASW covers a range of 6.5 – 37 Hz, having an overlapping zone with the HRFK Love data. The HRFK Love data reached as low as 0.7 Hz with a phase velocity of 680 m/sec.

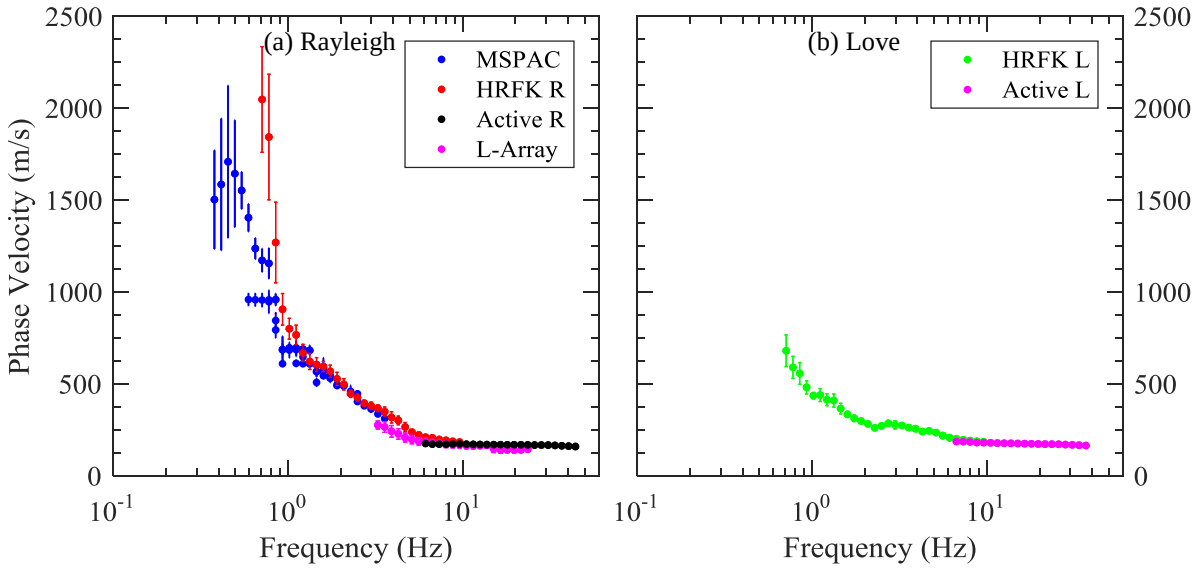

Figure 31. Composite experimental dispersion data shown for the HENM site (a) Rayleigh and (b) Love.

In Figure 32 (a) and (b), the experimental dispersion data and the 1000 lowest misfit theoretical dispersion curves along with their counted median dispersion curve are shown for Rayleigh and Love waves, respectively. The Rayleigh active MASW and L-Array data resolved

fundamental mode dispersion data from 3.5 – 45 Hz. The MSPAC data from 0.85 – 1 Hz were also resolved as fundamental mode. The HRFK Rayleigh data were resolved as first higher mode from 0.85 – 2.5 Hz. The Love active MASW and HRFK Love data were resolved as fundamental mode dispersion data from 2.2 – 37 Hz. After numerous iterations to assign the correct modes to the experimental data and removing the effective mode, the final 2 million model inversion had a minimum misfit of 0.52. The median of the 1000 best HENM site V_S profiles was used to compute the theoretical fundamental mode Rayleigh wave ellipticity as shown in Figure 32 (c). The theoretical ellipticity peak, $f_{0,thr}$ was determined to be 0.367 Hz, which is within one standard deviation of the experimental HVSR peak of 0.365 Hz.

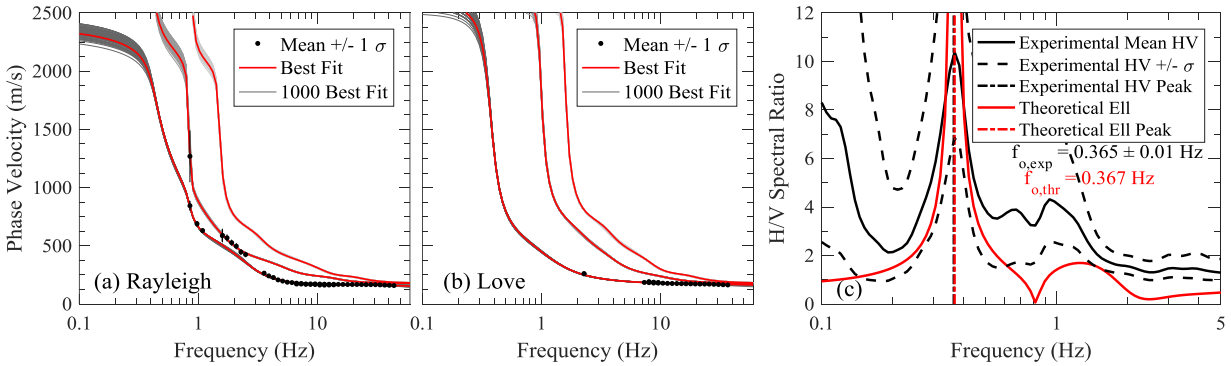

Figure 32. Experimental dispersion data and theoretical fits for the 1000 lowest misfit V_S profiles at HENM are shown for (a) Rayleigh wave and (b) Love wave, respectively. The experimental HVSR curve and the theoretical ellipticity curve associated with the median V_S profile are shown in (c).

The V_S results from the HENM site inversions are shown in Figure 33. The one thousand best V_S profiles along with their counted median are shown. In addition, the V_S profiles from Ramirez-Guzman *et al.*, 2012 (CUSVM), and Romero and Rix, 2005 lowland V_S profiles are shown for comparison. Reference V_S profiles from Lin et al., 2014 for several materials are added.

From the Vs profiles shown in the Figure 33a, the Romero and Rix, 2005 lowland V_S profile is stiffer than the SWM and CUSVM V_S profiles down to a depth of approximately 35 m in the Quaternary layer. The CUSVM and SWM V_S profiles lie between the soft soil and dense sand reference profiles, which is consistent for the soft alluvium found in Quaternary layer. Both V_S profiles are comparable from approximately 60 – 125 m until the SWM V_S profile resolves the Memphis sand layer. The CUSVM V_S profile resolved the Memphis sand layer at a shallow depth of around 65 m with a V_S of 445 m/sec, whereas the SWM V_S profile resolved the Memphis sand layer around 120 – 140 m deep with a velocity range of 600 – 630 m/sec. The CUSVM and Romero and Rix, 2005 lowland V_S profiles are 7 – 20% softer than the SWM V_S profile in the depth range of 120 – 380 m. The CUSVM V_S profile resolves the Upper Cretaceous layer at 390 m with a V_S of 900 m/sec, whereas the SWM V_S profile resolves the Upper Cretaceous layer at a deeper depth of around 410 m with a V_S of 750 – 810 m/sec. The bedrock V_S ranges from 2500 – 2700 m/sec for the HENM V_S profile, whereas the CUSVM has a bedrock V_S of 2000 m/sec.

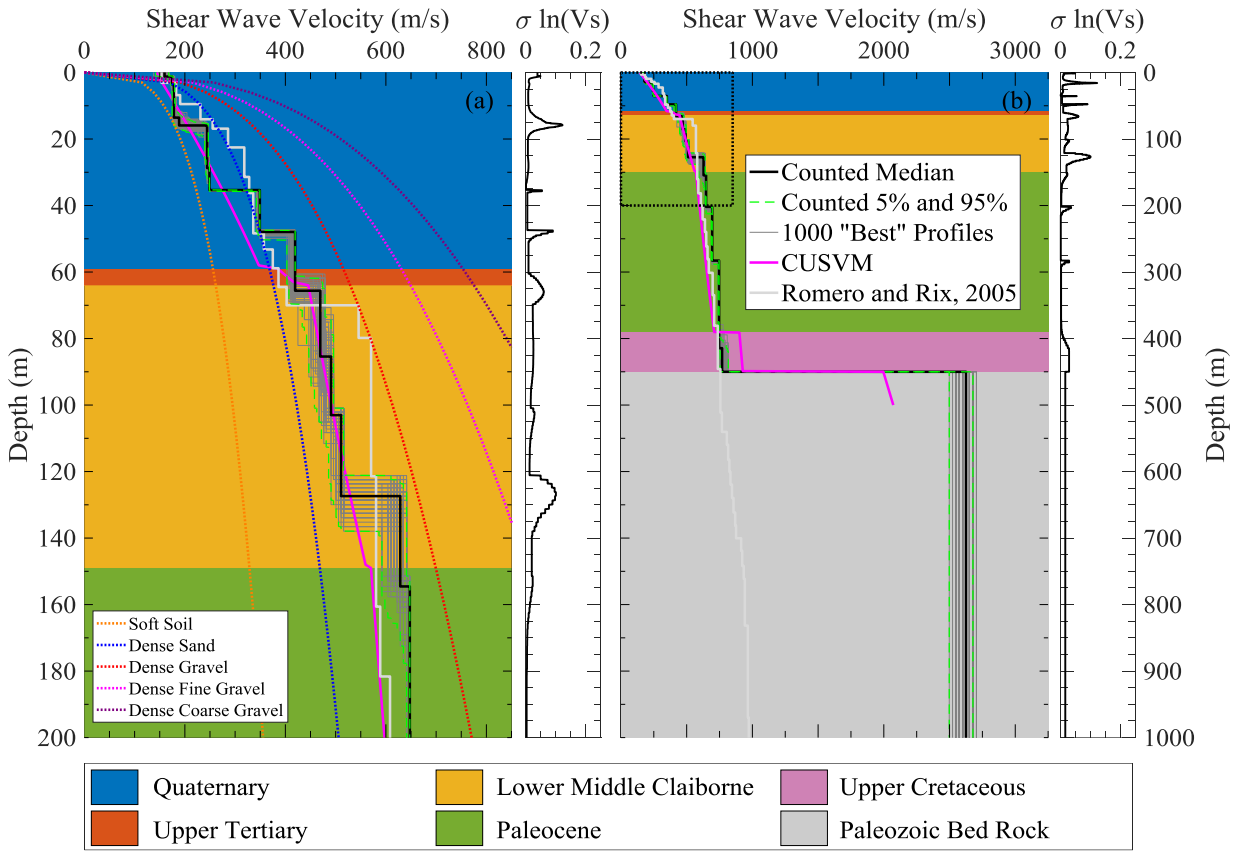

Figure 33. One thousand best V_S profiles along with their counted median for HENM site are shown. The V_S profiles from Ramirez-Guzman *et al.*, 2012 (CUSVM) and Romero and Rix, 2005 lowland profiles are also included for comparison. The σln(Vs) is for the HENM profiles demonstrating the uncertainty in V_S. The blue dashed lines represent the counted 5th and 95th percentile V_S confidence interval for the 1000 HENM profiles. Reference V_S profiles from Lin *et al.*, 2014 for different soil types are also included. Geologic unit boundaries from CUSVM are shown for HENM with different color codes.

(vi) **LPAR:** The LPAR seismic station is situated in Poinsett County, Arkansas. Geologically this site is located in the lowland part of the Mississippi Embayment. The surface deposits at this site are Holocene age and the site has a bedrock depth of 840 m (Ramirez-Guzman *et al.*, 2012). At this site, surface wave data were collected using a 46 m linear active MASW array, a 60x55 m L-array, and circular arrays of diameter 50 m, 200 m, and 500 m.

The experimental dispersion data for the Rayleigh and Love wave data collected at the LPAR site are shown in Figure 34 (a) and (b), respectively. The collected Rayleigh active MASW data covers a frequency range from 7.5 – 45 Hz, and overlaps with the L-Array data, showing no sign of near field effects. Some experimental data points from the HRFK Rayleigh have lower phase velocity than the active MASW around 9.5 Hz, which might be due to failure to eliminate some data beyond array resolution limit (Wathelet *et al.*, 2008). These data are later removed during the inversion processing. The L-Array data fit well with the MSPAC and HRFK Rayleigh

data and cover a frequency range from 3.3 – 9.5 Hz, with an overlapping zone around 3.5 Hz. The MSPAC and HRFK Rayleigh have similar trends. The maximum phase velocity was reached by HRFK Rayleigh data at 0.5 Hz, with a phase velocity of 2300 m/sec. The Love active MASW data cover a frequency range of 4.2 – 45 Hz and overlap with some part of the HRFK Love data. Love HRFK also have the same trend of lower phase velocity than the active MASW data near 9.5 Hz. The lowest frequency reached by the HRFK Love is around 0.8 Hz, with a phase velocity of 690 m/sec.

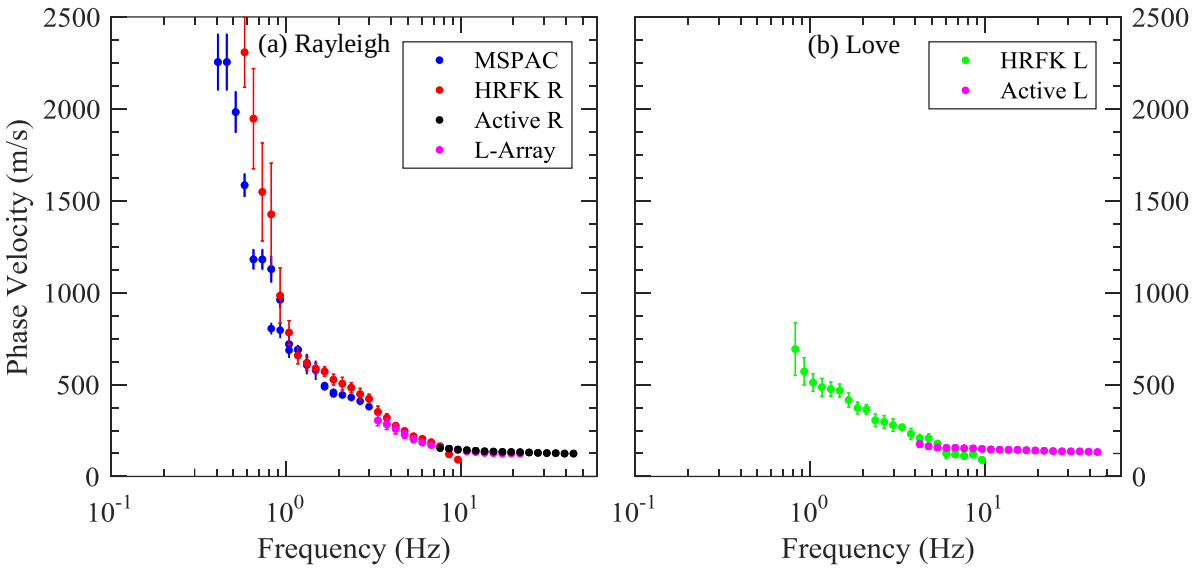

Figure 34. Composite experimental dispersion data shown for LPAR site the (a) Rayleigh and (b) Love.

In Figure 35 (a) and (b), the experimental dispersion data and the 1000 lowest misfit theoretical curves along with their counted median dispersion curves are shown for Rayleigh and Love waves, respectively. The Rayleigh active MASW, L-array, HRFK Rayleigh and MSPAC data resolved the fundamental mode from 1.6 – 45 Hz. Some data points from MSPAC were resolved as first higher mode from 0.51 – 0.65 Hz. All Love active MASW data resolved the fundamental mode. After numerous iterations to assign the correct modes to experimental data and removing the effective mode, the final 2 million model inversion had a minimum misfit of 0.33. The median of the 1000 best LPAR site V_S profiles was used to compute the theoretical fundamental mode Rayleigh wave ellipticity as shown in Figure 35 (c). The theoretical ellipticity peak, $f_{0,thr}$ was determined to be 0.242 Hz, which is within one standard deviation of the experimental HVSR peak of 0.241 Hz.

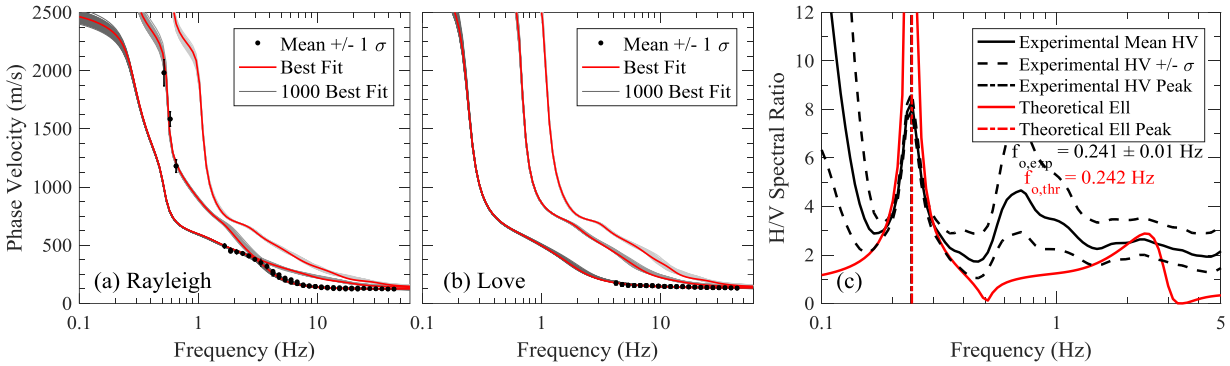

Figure 35. Experimental dispersion data and theoretical fits for the 1000 lowest misfit V_S profiles at LPAR are shown for (a) Rayleigh wave and (b) Love wave, respectively. The experimental HVSR curve and the theoretical ellipticity curve associated with the median V_S profile are shown in (c).

The V_S results from the LPAR site inversions are shown in Figure 36. The one thousand best V_S profiles along with their counted median are shown. In addition, the V_S profiles from Ramirez-Guzman *et al.*, 2012 (CUSVM), and Romero and Rix, 2005 lowland V_S profiles are shown for comparison. Reference V_S profiles from Lin et al., 2014 for several materials are added.

From the Vs profiles in the Figure 36a, the SWM and CUSVM V_S profiles lie between the soft soil and dense sand reference curves, which is consistent with the soft alluvium in Quaternary layer. However, the SWM V_S profile surpasses the dense sand curve around 30 m, which might be an indication of Upper Tertiary layer in the SWM V_S profile. The SWM and Romero and Rix, 2005 lowland V_S profiles match well down to 30 m, whereas the CUSVM is 7 – 20% softer than the other V_S profiles in the depth range of 10 m to 90 m. The CUSVM resolves the Memphis sand layer at a depth of 90 m with a V_S of 445 m/sec, which the SWM resolves around 170 m with a V_S of 670 m/sec. The CUSVM V_S profile is consistently softer throughout the Paleocene unit, where the SWM and Romero and Rix, 2005 match for the most part, with the CUSVM 5 – 16% softer in the Paleocene layer. The Upper Cretaceous layer is resolved around 650 m deep in the SWM V_S profile, whereas the CUSVM V_S profile resolves the layer around 690 m. The bedrock V_S ranges from 2700 – 2900 m/sec for the SWM, whereas the CUSVM demonstrates a bedrock V_S of 1325 m/sec.

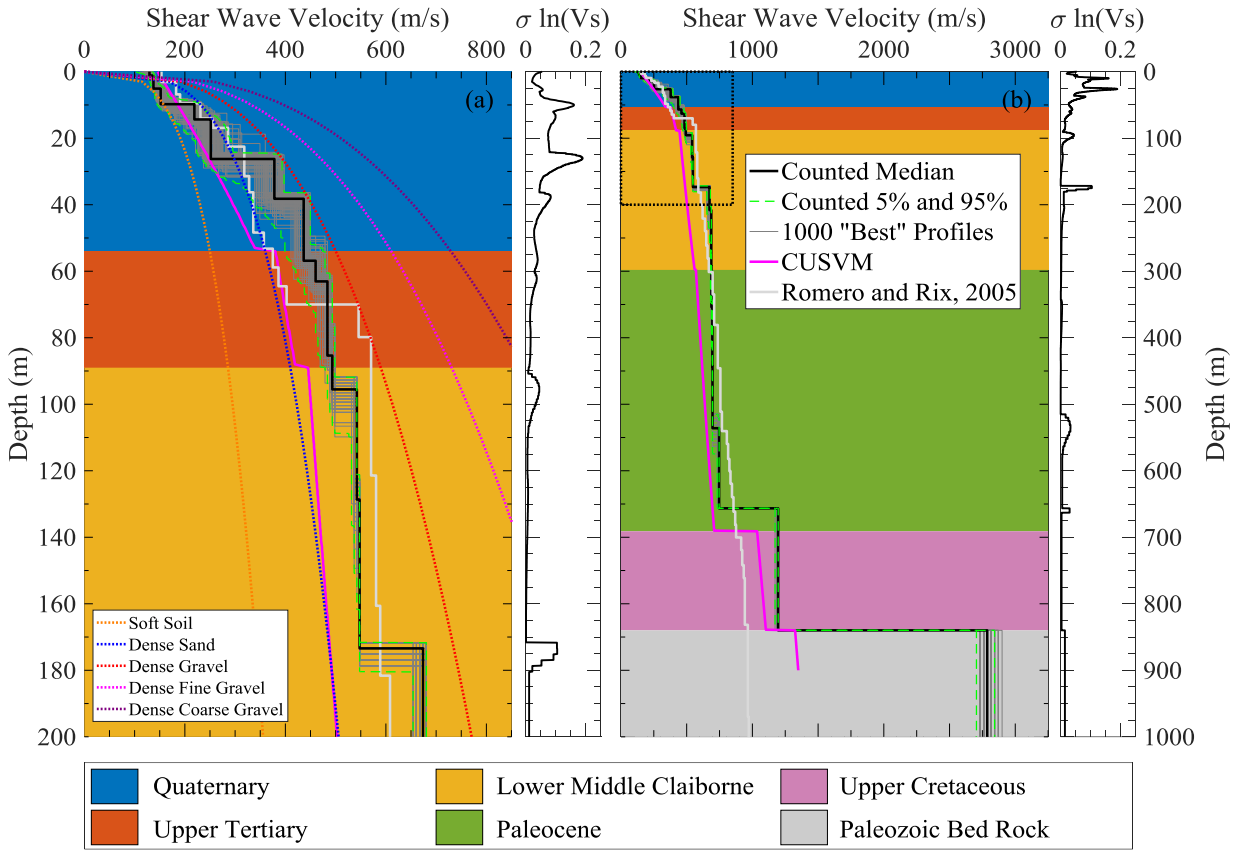

Figure 36. One thousand best V_S profiles along with their counted median for LPAR site are shown. The V_S profiles from Ramirez-Guzman *et al.*, 2012 (CUSVM) and Romero and Rix, 2005 lowland profiles are also included for comparison. The σln(Vs) is for the LPAR profiles demonstrating the uncertainty in V_S. The blue dashed lines represent the counted 5th and 95th percentile V_S confidence interval for the 1000 LPAR profiles. Reference V_S profiles from Lin *et al.*, 2014 for different soil types are also included. Geologic unit boundaries from CUSVM are shown for LPAR with different color codes.

(vii) **PARM:** The PARM seismic station is situated in New Madrid County, Missouri. Geologically this site is located in the lowland part of the Mississippi Embayment. The surface deposits at this site are Holocene age and the site has a bedrock depth of 427 m (Ramirez-Guzman *et al.*, 2012). At this site, surface wave data were collected using a 46 m linear active MASW array, a 60x55 m L-array, and circular arrays of diameter 50 m, 200 m, and 500 m.

The experimental dispersion data for the Rayleigh and Love wave data collected at the PARM site are shown in Figure 37 (a) and (b), respectively. The Rayleigh active MASW data covers a frequency range from 5.5 – 45 Hz, with an overlapping zone with the L-Array data. The L-array data and the high frequency HRFK Rayleigh data have a hump near 6 Hz, which were later detected as the effective mode data in the inversion processing and were removed. The HRFK Rayleigh data have similar trend to the MSPAC from 3 Hz down to frequency as low as 0.3 Hz. The lowest frequency resolved was 0.3 Hz using the MSPAC, with a phase velocity of 2200 m/sec. The Love active MASW covers a frequency range from 6.8 – 48 Hz and overlaps with the HRFK Love curve. The HRFK Love data reach as low as 0.7 Hz with a phase velocity of 690 m/sec.

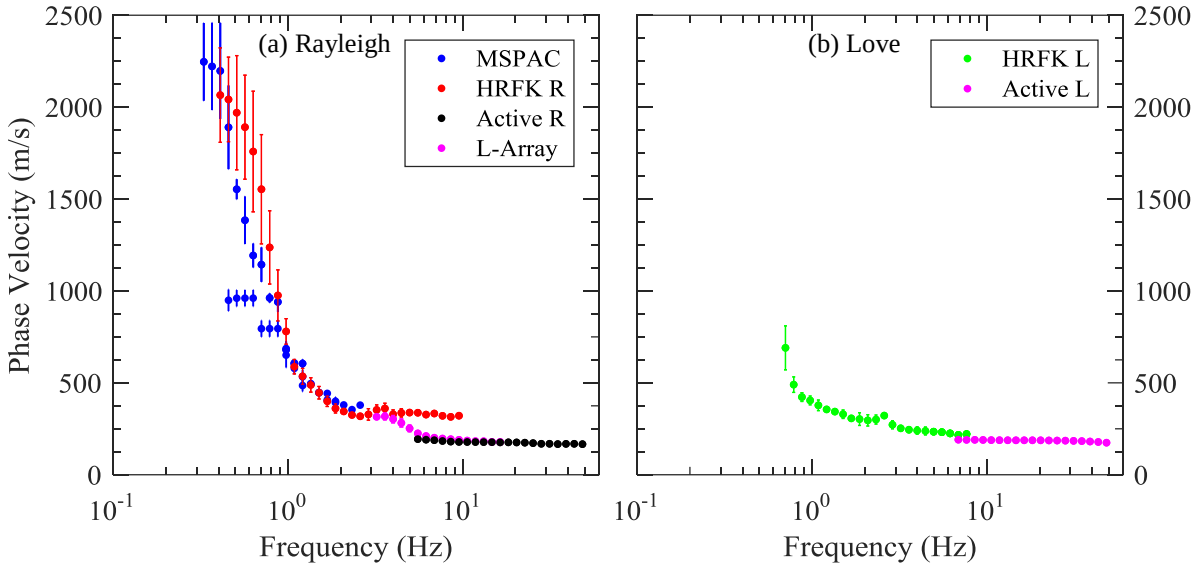

Figure 37. Composite experimental dispersion data shown for the PARM site the (a) Rayleigh and (b) Love.

In Figure 38 (a) and (b), the experimental dispersion data and the 1000 lowest misfit theoretical curve along with their counted median dispersion curve are shown for Rayleigh and Love wave data, respectively. The Rayleigh active MASW data were resolved as fundamental mode. Most of the L-array, and some part of HRFK Rayleigh data (around 6 Hz) were removed due to it being resolved as effective mode data. The Rayleigh HRFK data ranging from 0.9 – 2.5 Hz were resolved as fundamental mode. Data points for MSPAC and HRFK from 0.7 – 0.87 Hz were identified as first higher mode. Active Love and Love HRFK data were identified as fundamental mode ranging from 0.7 – 48 Hz. After numerous iterations to assign the correct modes to the experimental data and eliminating the effective mode, the final 2 million model inversion had a minimum misfit of 0.43. The median of the 1000 best PARM site V_S profiles was used to compute the theoretical fundamental mode Rayleigh wave ellipticity as shown in Figure 38 (c). The theoretical ellipticity peak, $f_{0,thr}$ was determined to be 0.385 Hz, which is within one standard deviation of the experimental HVSR peak of 0.383 Hz.

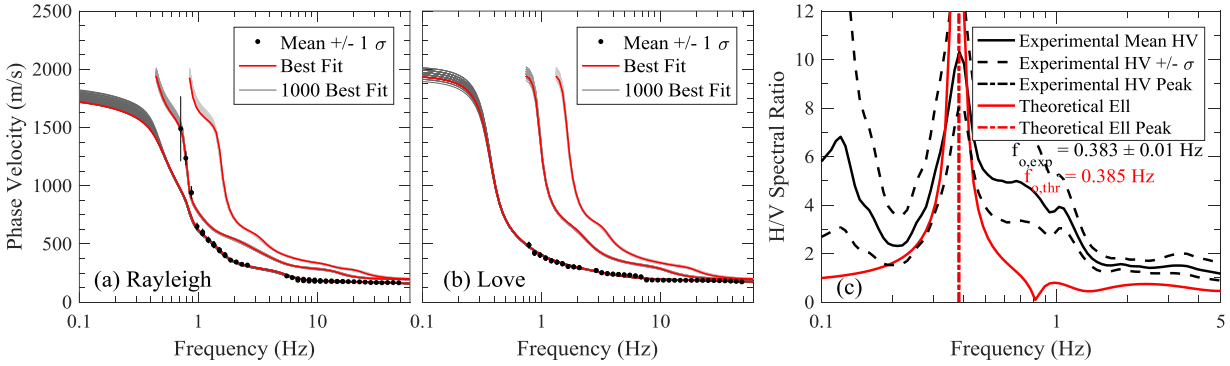

Figure 38. Experimental dispersion data and theoretical fits for the 1000 lowest misfit V_S profiles at PARM are shown for (a) Rayleigh wave and (b) Love wave, respectively. The experimental HVSR curve and the theoretical ellipticity curve associated with the median V_S profile are shown in (c).

The V_S results from the PARM site inversions are shown in Figure 39. The one thousand best V_S profiles along with their counted median are shown. In addition, the V_S profiles from Ramirez-Guzman *et al.*, 2012 (CUSVM), and Romero and Rix, 2005 lowland V_S profiles are shown for comparison. Reference V_S profiles from Lin et al., 2014 for several materials are added.

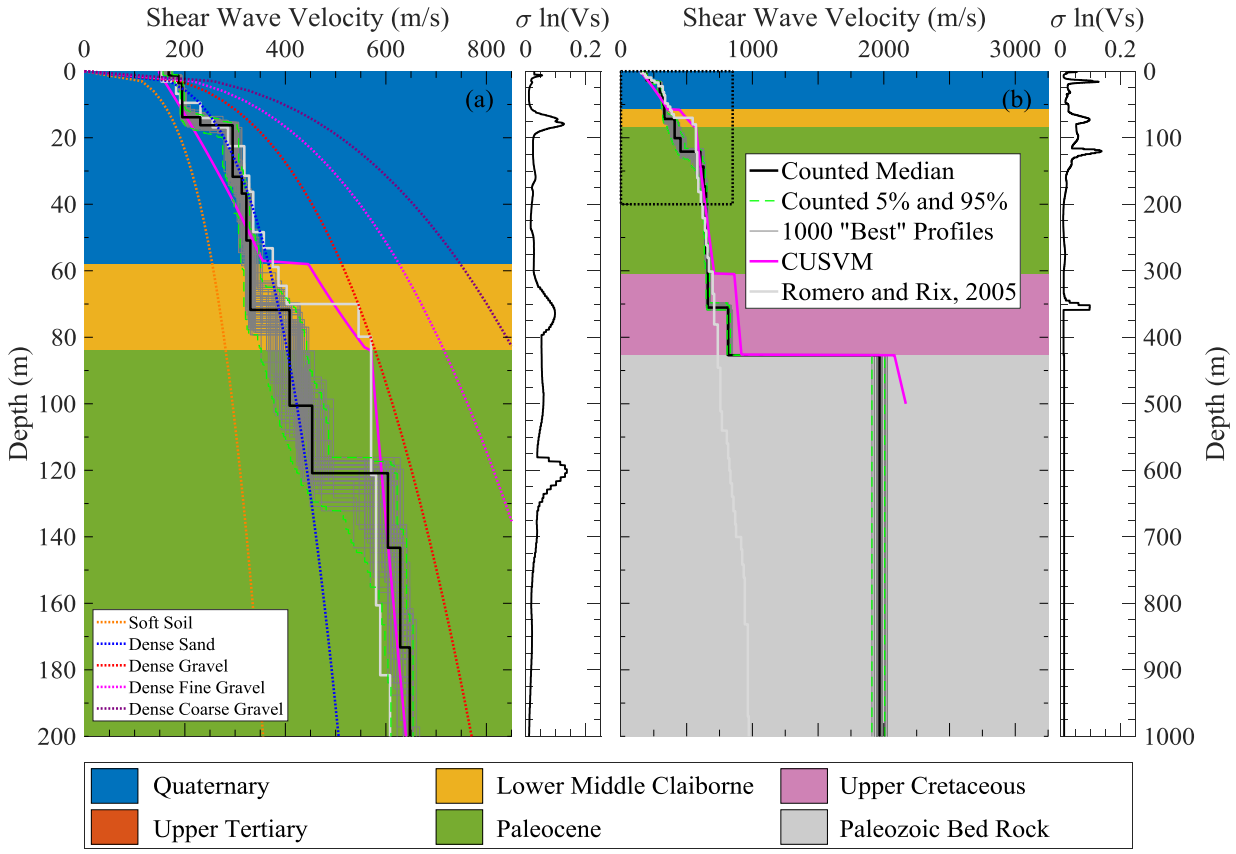

Figure 39. One thousand best V_S profiles along with their counted median for PARM site are shown. The V_S profiles from Ramirez-Guzman *et al.*, 2012 (CUSVM) and Romero and Rix, 2005 lowland profiles are also included for comparison. The σln(Vs) is for the PARM profiles demonstrating the uncertainty in V_S. The blue dashed lines represent the counted 5^{th} and 95^{th} percentile V_S confidence interval for the 1000 PARM profiles. Reference V_S profiles from Lin *et al.*, 2014 for different soil types are also included. Geologic unit boundaries from CUSVM are shown for PARM with different color codes.

For the Vs profiles in Figure 39 (a), the SWM and Romero and Rix, 2005 lowland V_S profiles are in good agreement down to around 60m. The CUSVM V_S profile resolves the Memphis sand layer around a depth of 60 m and is stiffer than the other two V_S profiles. The SWM V_S profile indicates the Quaternary layer continues down to 70 m, and until this depth lie between the soft soil and dense sand reference curves. The SWM V_S profile resolves the Memphis sand layer around 120 m with a V_S of 590 – 630 m/sec. The SWM V_S profile lies between the dense sand and dense gravel from 120 m, which is consistent with the stiff sand formation in Lower Middle Claiborne. Approximately, from 120 – 300 m, the CUSVM and SWM V_S profiles are consistent. The CUSVM V_S profile resolves the Upper Cretaceous layer around 300 m with a velocity of 862 m/sec, which makes the profile about 30% stiffer than the SWM and Romero and Rix, 2005 lowland V_S profiles at this depth. The SWM V_S profile resolves the Upper Cretaceous layer around

350 m with a V_S of approximately 830 m/sec. The bedrock V_S ranges from 1900 – 2000 m/sec in the SWM V_S profile, whereas the CUSVM has a bedrock V_S of 2080 m/sec.

(viii) **PEBM:** The PEBM seismic station is situated in Pemiscot County, Missouri. Geologically this site is located in the lowland part of the Mississippi Embayment. The surface deposits at this site are Holocene age and the site has a bedrock depth of 764 m (Ramirez-Guzman *et al.*, 2012). At this site, surface wave data were collected using a 46 m linear active MASW array, a 60x55 m L-array, and circular arrays of diameter 50 m, 200 m, and 500 m.

The experimental dispersion data for the Rayleigh and Love wave data collected at the PEBM site are shown in Figure 40 (a) and (b), respectively. The Rayleigh active MASW, L-Array, and HRFK have similar trend and cover a frequency range from 0.9 – 45 Hz. The HRFK Rayleigh data reaches a low frequency of 0.3 Hz with a phase velocity of 2500 m/sec. The MSPAC data are scattered in the low frequency range, but follows the HRFK Rayleigh data trend. The Love active MASW data covers a range from 4.5 – 45 Hz and overlaps with the Love HRFK around 5 Hz. The Love HRFK data extends down to 0.8 Hz with phase velocity of 570 m/sec.

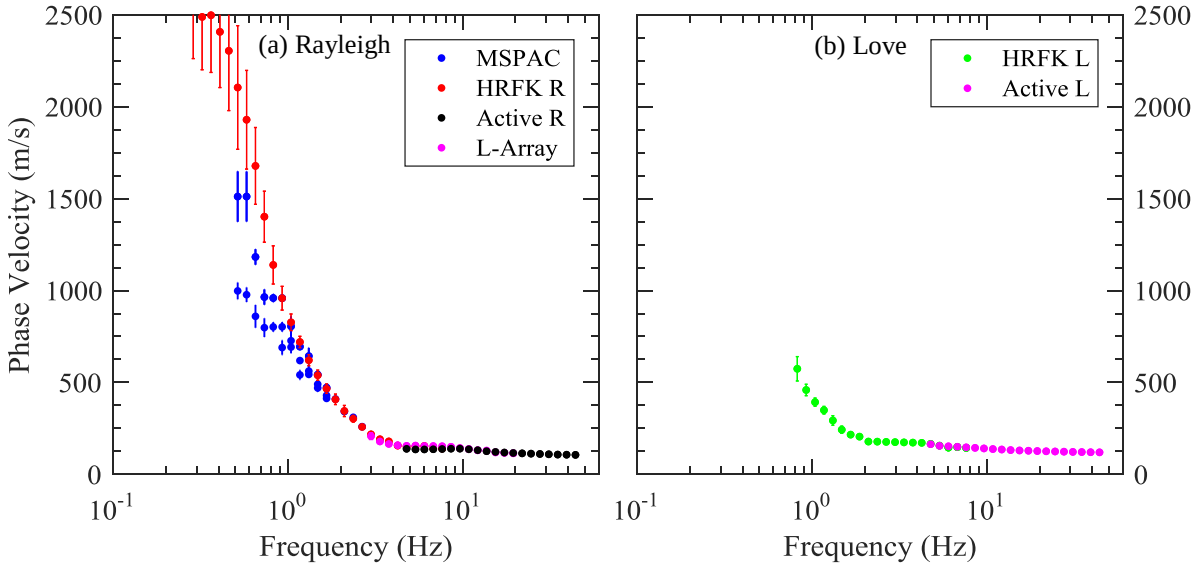

Figure 40. Composite experimental dispersion data shown for the PEBM site, (a) Rayleigh and (b) Love.

In Figure 41 (a) and (b), the experimental dispersion data and the 1000 lowest misfit theoretical curves along with their counted median dispersion curve are shown for Rayleigh and Love waves, respectively. The Rayleigh active MASW, L-Array, and HRFK data resolved the fundamental mode from 45 Hz down to 1.6 Hz. The MSPAC resolved the fundamental mode to around 1.6 Hz. MSPAC and Rayleigh HRFK data were resolved as first higher mode from 1.5 Hz, down to 0.45 Hz. The Love active MASW and HRFK data were resolved as fundamental mode for a frequency range from 0.9 – 45 Hz. After numerous iterations to assign the correct modes to the experimental data and removing the effective mode data, the final 2 million model inversion had a minimum misfit of 0.29. The median of the 1000 best PEBM site V_S profiles was used to compute the theoretical fundamental mode Rayleigh wave ellipticity as shown in Figure 41 (c).

The theoretical ellipticity peak, $f_{0,thr}$ was determined to be 0.265 Hz, which is within one standard deviation of the experimental HVSR peak of 0.267 Hz.

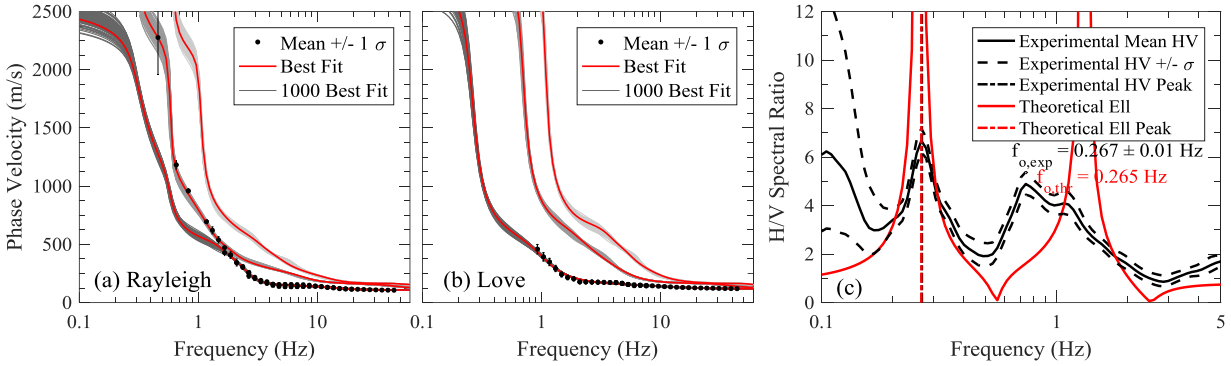

Figure 41. Experimental dispersion data and theoretical fits for the 1000 lowest misfit V_S profiles at PEBM are shown for (a) Rayleigh wave and (b) Love wave, respectively. The experimental HVSR curve and the theoretical ellipticity curve associated with the median V_S profile are shown in (c).

The V_S results from the PEBM site inversions are shown in Figure 42. The one thousand best V_S profiles along with their counted median are shown. In addition, the V_S profiles from Ramirez-Guzman *et al.*, 2012 (CUSVM), and Romero and Rix, 2005 lowland V_S profiles are shown for comparison. Reference V_S profiles from Lin et al., 2014 for several materials are added.

For the Vs profiles in the Figure 42 (a), the SWM V_S profile is softer than the reference soft soil curve from 10 – 20 m, which is due to the low phase velocity experimental data at frequencies higher than 5 Hz as shown in Figure 41 (a). The SWM and Romero and Rix, 2005 lowland V_S profiles lie between the dense gravel and dense sand reference curve from 20 – 70 m depth, indicating a shallower start to the Upper Tertiary than the CUSVM V_S profile. The V_S at 20 – 70 m deep is consistent with the stiff clay and sand formation found in the Upper Tertiary layer. The CUSVM resolved the Memphis sand layer around a depth of 120 m with a velocity of 445 m/sec, whereas the SWM V_S profile resolved the layer at a depth of 120 – 140 m with a velocity of 600 – 650 m/sec. Due to the lower Memphis sand velocity, the CUSVM V_S profile is softer from 120 – 700 m deep with a Vs of 18 – 20% softer than the SWM and Romero and Rix, 2005 lowland V_S profiles. Both CUSVM and SWM V_S profiles resolved the Upper Cretaceous layer around 630 m. The Upper Cretaceous velocity of CUSVM and median SWM V_S profiles are 1000 and 1100 m/sec at 700 m. The bedrock V_S ranges from 2500 – 2900 m/sec for the SWM, whereas the CUSVM demonstrates a bedrock V_S of 1980 m/sec.

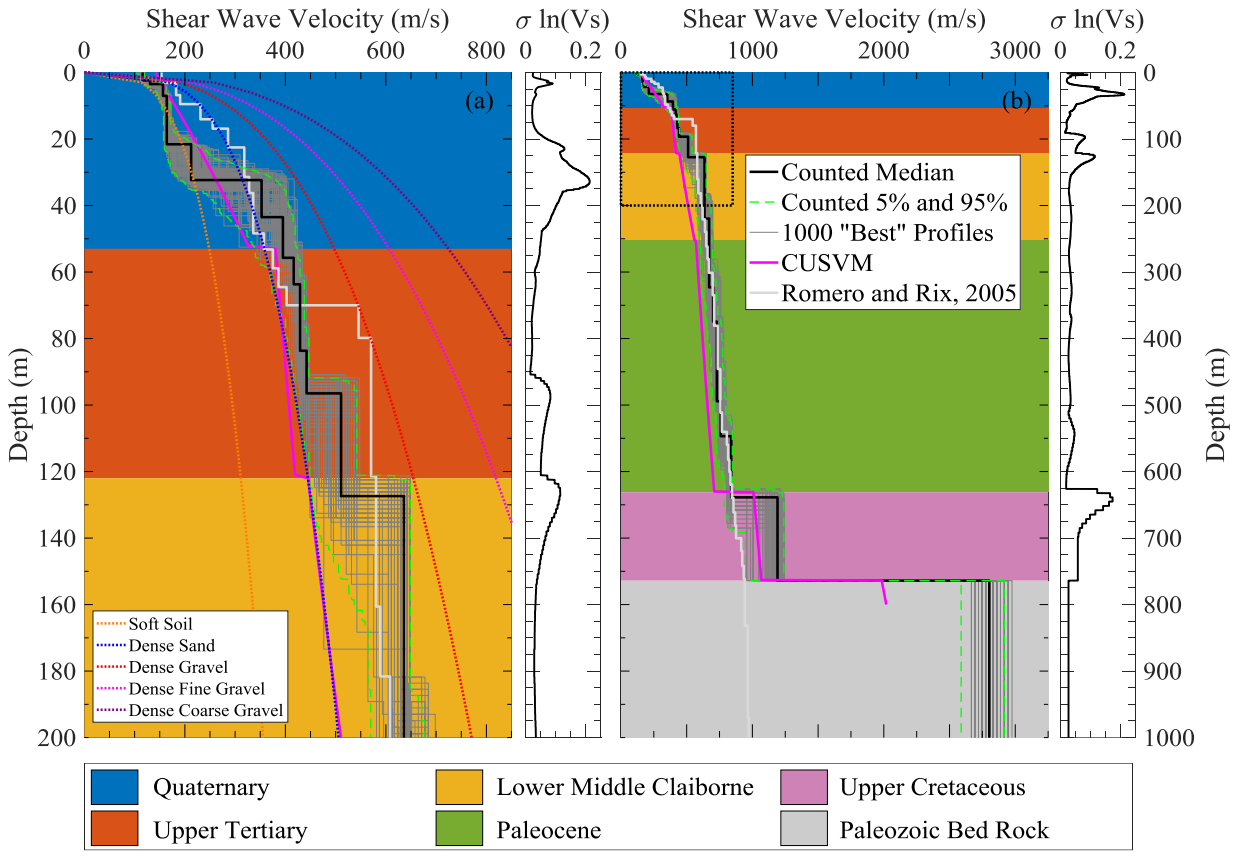

Figure 42. One thousand best V_S profiles along with their counted median for PEBM site are shown. The V_S profiles from Ramirez-Guzman *et al.*, 2012 (CUSVM) and Romero and Rix, 2005 lowland profiles are also included for comparison. The σln(Vs) is for the PEBM profiles demonstrating the uncertainty in V_S. The blue dashed lines represent the counted 5th and 95th percentile V_S confidence interval for the 1000 PEBM profiles. Reference V_S profiles from Lin *et al.*, 2014 for different soil types are also included. Geologic unit boundaries from CUSVM are shown for PEBM with different color codes.

(ix) **PVMO:** The PVMO seismic station is located in Pemiscot County, Missouri. Geologically this site is located in the lowland part of the Mississippi Embayment. The surface deposits at this site are Holocene age and the site has a bedrock depth of 591 m (Ramirez-Guzman *et al.*, 2012). At this site, surface wave data were collected using a 46 m linear active MASW array, a 60x55 m L-array, and circular arrays of diameter 50 m, 200 m, and 500 m.

The experimental dispersion data for the Rayleigh and Love wave data collected at the PVMO site are shown in Figure 43 (a) and (b), respectively. The Rayleigh active MASW data covers a frequency range from 8.8 – 45 Hz, and overlaps with the L-Array from 8.8 – 22 Hz with no sign of near-field effects present. The L-Array data covers a range from 2.5 – 8.8 Hz and has similar trend to the HRFK Rayleigh data. The MSPAC and HRFK Rayleigh data have similar trend down to 0.45 Hz. The lowest frequency reached by the HRFK data is 0.3 Hz with a phase velocity of 2200 m/sec. The Love active MASW data covers a frequency range from 7 – 45 Hz. The Love active MASW data from 20 - 45 Hz appear to be effective/higher mode as it has a higher

phase velocity than other portions of the dispersion data. However, the Love active MASW data around 7 Hz has a lower phase velocity then the Love HRFK, though the trend does not appear to be due to near field effects. The HRFK Love data extends down to 0.65 Hz with a phase velocity of 680 m/sec.

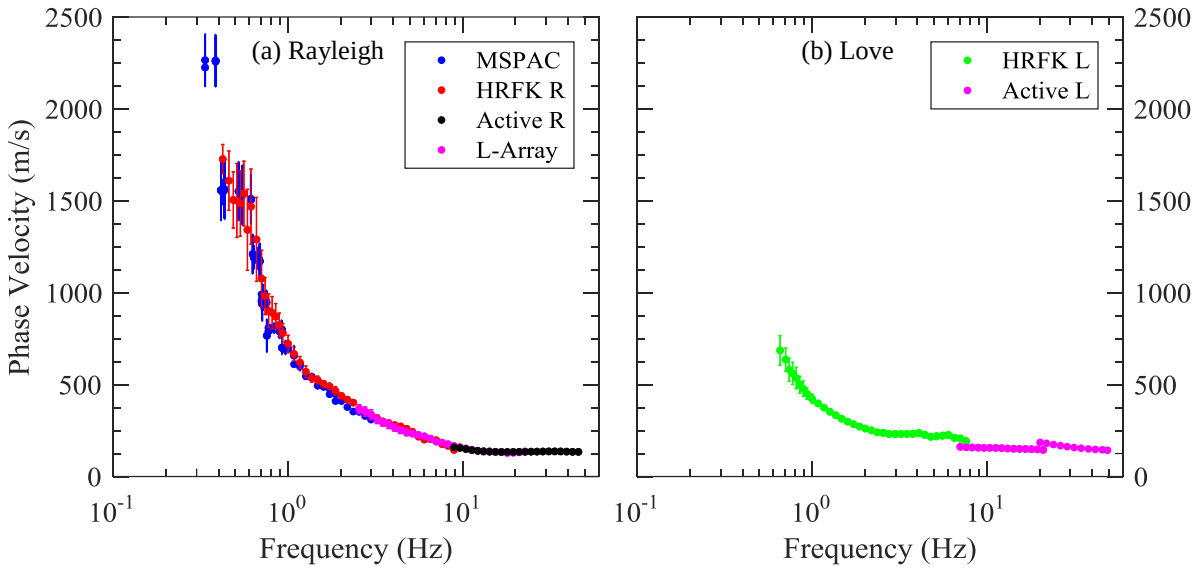

Figure 43. Composite experimental dispersion data shown for the PVMO site, (a) Rayleigh and (b) Love.

In Figure 44 (a) and (b), the experimental dispersion data and the 1000 lowest misfit theoretical curves along with their counted median dispersion curve are shown for Rayleigh and Love wave, respectively. The Rayleigh active MASW, L-Array, and HRFK Rayleigh data resolved the fundamental mode from 1.5 – 45 Hz. The MSPAC and HRFK Rayleigh data were resolved as first higher mode from 0.6 – 0.7 Hz. The Love active MASW data from 20 – 45 Hz were resolved first higher mode. The HRFK Love, and Love active MASW data were resolved fundamental mode from 0.9 – 20 Hz. After numerous iterations to assign the correct modes to experimental data and eliminating the effective mode, the final 2 million model inversion had a minimum misfit of 0.32. The median of the 1000 best PVMO site V_S profiles was used to compute the theoretical fundamental mode Rayleigh wave ellipticity as shown in Figure 44 (c). The theoretical ellipticity peak, $f_{0,thr}$ was determined to be 0.291 Hz, which is within one standard deviation of the experimental HVSR peak of 0.291 Hz.

The V_S results from the PVMO site inversions are shown in Figure 45. The one thousand best V_S profiles along with their counted median are shown. In addition, the V_S profiles from Ramirez-Guzman *et al.*, 2012 (CUSVM), and Romero and Rix, 2005 lowland V_S profiles are shown for comparison. Reference V_S profiles from Lin et al., 2014 for several materials are added.

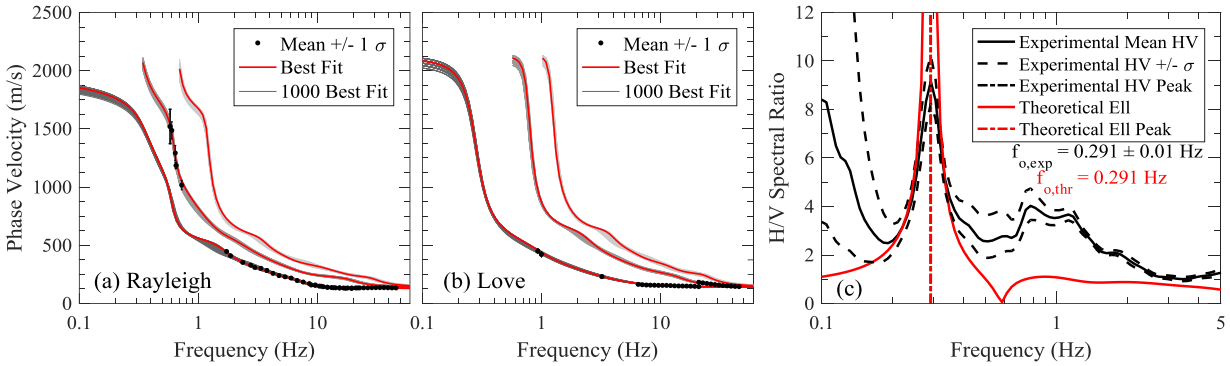

Figure 44. Experimental dispersion data and theoretical fits for the 1000 lowest misfit V_S profiles at PVMO are shown for (a) Rayleigh wave and (b) Love wave, respectively. The experimental HVSR curve and the theoretical ellipticity curve associated with the median V_S profile are shown in (c).

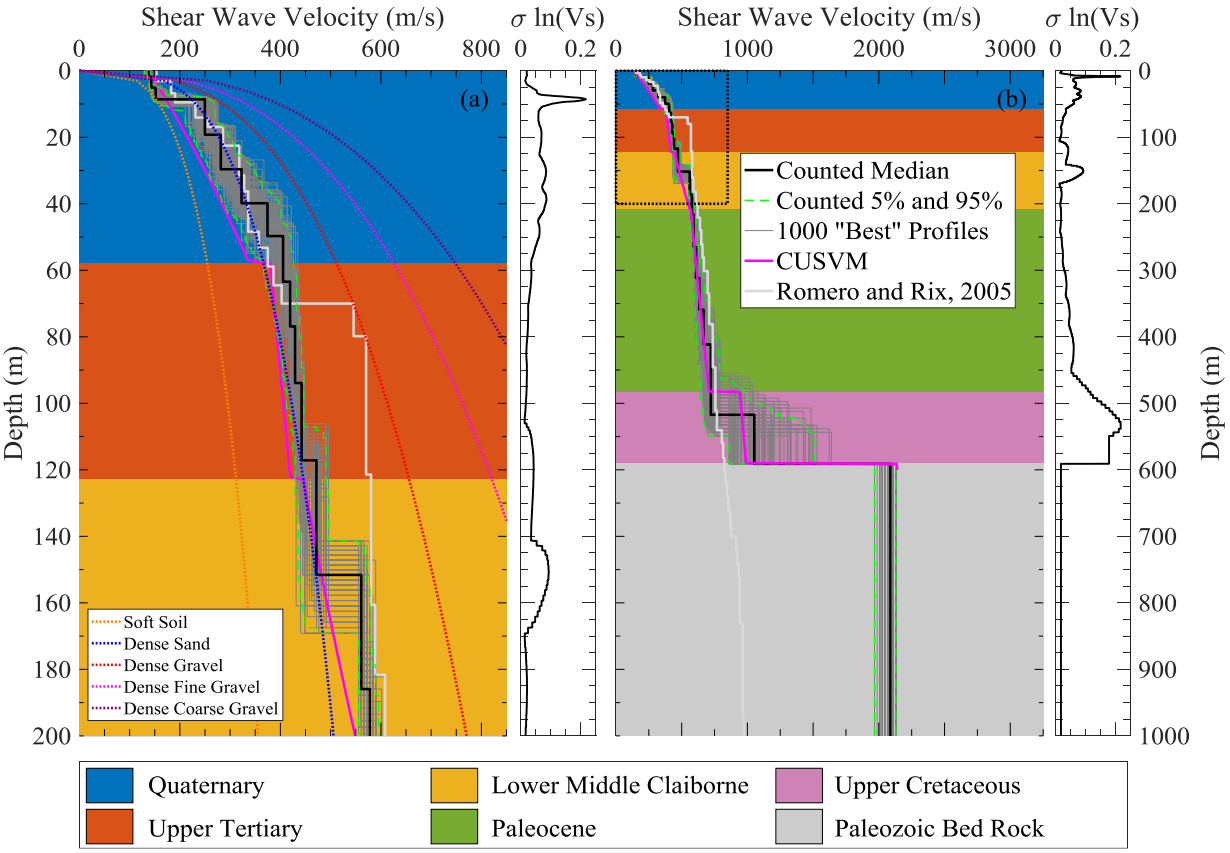

Figure 45. One thousand best V_S profiles along with their counted median for PVMO site are shown. The V_S profiles from Ramirez-Guzman *et al.*, 2012 (CUSVM) and Romero and Rix, 2005 lowland profiles are also included for comparison. The σln(Vs) is for the PVMO profiles demonstrating the uncertainty in V_S. The blue dashed lines represent the counted 5th and 95th percentile V_S confidence interval for the 1000 PVMO profiles. Reference V_S profiles from Lin *et al.*, 2014 for different soil types are also included. Geologic unit boundaries from CUSVM are shown for PVMO with different color codes.

For the Vs profiles in Figure 45 (a), the SWM and Romero and Rix, 2005 lowland V_S profiles have similar trends from surface down to 70 m deep. In the Upper Tertiary layer, all V_S profiles lie between the dense sand and dense gravel reference curve, which is consistent with the stiff clay and sand formation in this layer. The CUSVM V_S profile resolves the Memphis sand depth around 125 m with a velocity of 445 m/sec. The SWM V_S profile also resolves the Memphis sand close to the CUSVM at 140 – 160 m deep, with a velocity of 580 – 610 m/sec. The CUSVM V_S profile is softer than the other two V_S profile until the Paleocene layer. All three V_S profiles are consistent in the Paleocene layer. The CUSVM V_S profile resolves the Upper Cretaceous layer around 480 m with a velocity of 950 m/sec. The SWM V_S profile resolves the Upper Cretaceous layer around 450 – 530 m with velocity of 1000 – 1600 m/sec. The bedrock V_S for SWM ranges from 1950 – 2130 m/sec for the PVMO, whereas the CUSVM demonstrates a bedrock V_S of 2130 m/sec.

A summary of the V_{S30}, median formation depth of the Memphis sand layer, and median formation velocity of the Memphis sand layer at each site is provided in the Table 3. The average Memphis sand depth from the SWM V_S profiles and CUSVM are 143±26 m, and 79±39 m, respectively. Average formation velocity of the Memphis sand determined from SWM is 623±21 m/sec.

The CUSSO downhole V_S profile and all SWM median V_S profiles developed in this study are provided in the Table 4.

Table 3. Summary of V_{S30}, median formation depth of the Memphis sand layer, and median formation velocity of the Memphis sand layer at each site.

Site/V_S Profile	V_{S30} (m/sec)	Median depth to Memphis sand (m)	Median formation velocity of Memphis sand (m/sec)
CUSSO	224	130	606
CUSSO (Downhole)	228	122	628
HBAR	240	127	624
HENM	204	127	629
LNXT	252	177	614
LPAR	205	173	674
PARM	231	121	604
PEBM	167	127	636
PVMO	213	142	606
TUMT	305	190	612

Conclusion

A combination of active and passive source surface wave measurements were made at nine seismic station sites located in the northern part of the Mississippi Embayment. Deep shear wave velocity profiles were developed at each site using a joint inversion of surface wave data and fundamental frequency of the site. Downhole measurement at the CUSSO site was conducted to validate the use of surface wave methods to develop deep shear wave velocity profiles in the embayment. The time averaged shear wave velocity from the surface wave methods was within

1.0% of the average downhole V_S. The ellipticity peaks and shear wave transfer function peaks calculated from the CUSSO surface wave method V_S lie within 0.1 – 6.3 % of the fundamental frequency of the site. The validated surface wave methodology was applied to the rest of the eight sites to develop deep V_S profiles. The Romero and Rix, 2005 lowland profile matched well in most of the depth ranges with the surface wave method V_S profiles. However, a shallow impedance contrast at 70 m provided by the Romero and Rix, 2005 lowland V_S profile was not observed in most of the surface wave method V_S profiles developed in this study. Seven out of nine V_S profiles from this study indicate that the Memphis sand depth is deeper than the depths suggested by the CUSVM. In addition, regardless of the depth of Memphis sand, the formation velocity of this layer in the CUSVM V_S profiles is always 445 m/sec. However, Vs profiles from this study indicate the Vs of the Memphis sand layer ranges from 604 – 674 m/sec. Also, a difference in depth to the Upper Tertiary and the Upper Cretaceous layer was often observed between the CUSVM V_S profiles and the surface wave method V_S profiles. It is planned to incorporate these detailed velocity profiles into the CUSVM to increase the accuracy of the model. This future model would be beneficial for understanding the seismic amplification and ground motion studies in the Mississippi Embayment.

Table 4. Median shear wave velocity profiles.

CUSSO (SWM)		CUSSO (Downhole)		HBAR		HENM		LNXT	
Depth (m)	V_S (m/s)	Depth (m)	V_S (m/s)	Depth (m)	V_S (m/s)	Depth (m)	V_S (m/s)	Depth (m)	V_S (m/s)
0	168	0	160	0.0	161	0	160	0	139
7	222	5	235	0.5	205	1	175	2	163
22	327	21	280	5	207	3.5	178	4	217
35.5	369	37	385	10.5	210	13.5	189	9	257
59	395	125	600	20.5	360	16	244	17	329
70.5	407	205	675	29.5	390	28.5	249	27.5	360
103	408	255	700	40.5	403	35.5	349	42	372
130	606	390	620	51.5	417	48	419	52	381
199	612	495	875	71	442	65.5	469	68.5	392
230	618	585	2500	85.5	469	85.5	491	82	404
270	657			112	508	103	511	107	423
298	687			127	624	127	629	149	472
362	694			203	643	155	648	177	614
420	701			333	663	202	694	234	639
493	859			410	676	283	747	307	678
585	2130			461	697	415	769	398	712
				552	747	450	2625	475	762
				618	1179			552	825
				754	2775			670	1360
								845	2826

Table 4 continued. Median shear wave velocity profiles.

LPAR		PARM		PEBM		PVMO		TUMT		TUMT Station	
Depth (m)	V_S (m/s)	Depth (m)	V_S (m/s)	Depth (m)	V_S (m/s)	Depth (m)	V_S (m/s)	Depth (m)	V_S (m/s)	Depth (m)	V_S (m/s)
0	130	0	168	0	116	0	140	0	147	0	113
1	137	1.5	187	2.5	131	2	143	1.5	183	1	161
5	152	3.5	195	3.5	156	5	149	4	287	3.5	287
10	219	14	231	7	164	8	247	9.5	339	10	333
14.5	252	16	295	21.5	212	21.5	281	16	378	19	353
26	378	31.5	313	32.5	353	30	336	28.5	405	29.5	378
38	436	37	322	43.5	395	38	363	42.5	419	41	428
57	460	51	330	55.5	417	53.5	390	53	438	53	451
63	484	72	408	63.5	429	64.5	415	69	451	64.5	469
85.5	493	101	453	83.5	442	75.5	438	81	469	81.5	489
95.5	542	121	604	96.5	511	92	484	102	481	100	491
129	548	143	629	127	636	143	606	144	511	151	496
173	674	173	648	220	671	168	612	190	612	179	576
208	687	274	661	323	701	188	618	239	624		
292	689	355	816	375	730	212	624	326	643		
354	696	427	1967	494	759	265	631	402	656		
443	697			547	839	300	637	475	683		
536	747			639	1191	370	656	569	704		
657	1196			764	2803	437	697	650	732		
840	2787					538	987	770	1029		
						591	2088	923	1948		

References

Asten, M. W. and Boore, D. M. (2005) Comparison of shear-velocity profiles of unconsolidated sediments near the Coyote borehole (CCOC) measured with fourteen invasive and non-invasive methods, Blind comparisons of shear-wave velocities at closely-spaced sites in San Jose, California, M. W. Asten and D. M. Boore (Editors), U.S. Geological Survey Open-File Report OFR 2005-1169 .

Aki, K., 1957. Space and time spectra of stationary stochastic waves, with special reference to microtremors, *Bulletin of Earthquake Research Institute* **35**, 415–456.

Barani, S., Ferrari, R., Ferretti, G., 2013. Influence of soil modeling uncertainties on site response, *Earthquake Spectra*, **29(3)**, 705–732

Bazzurro, P. and Cornell, C.A., 2004. Nonlinear soil-site effects in probabilistic seismic-hazard analysis, *Bull. Seism. Soc. Am.* **94**, 2110-2123.

Bettig, B., Bard, P.Y., Scherbaum, F., Riepl, J., Cotton, F., Cornou, C., and Hatzfield, D., 2001. Analysis of dense array noise measurements using the modified spatial auto correlation method (SPAC): application to the Grenoble area, *Bollettino de Geofisica Teoria e Applicata* **42(3-4)**, 281-304.

Boore, David M., et al., 2003. Estimated Ground Motion From the 1994 Northridge, California, Earthquake at the Site of the Interstate 10 and La Cienega Boulevard Bridge Collapse, West Los Angeles, California *Bull. Seism. Soc. Am.* **90(6)**, 2737–2751

Bradley, B.A., Quigley, M., and Van Dissen, R., Litchfield N.J., 2014. Ground motion and seismic rupture aspects of the 2010-2011 Canterbury earthquake sequence, *Earthquake Spectra* **30 (1)**, 1-15.

Brahana, J.V., Parks, W. S., and Gaydos, M. W., 1987. *Quality of Water from Freshwater Aquifers and Principal Well Fields in the Memphis Area*, Tennessee. USGS Water- Resources Investigations Report 87-4052.

Capon, J., 1969. High Resolution Frequency-Wavenumber Spectrum Analysis, in *Proceedings, IEEE* **57(8)**, 1408–1418.

Cox, B and Wood, C., 2011. Surface Wave Benchmarking Exercise: Methodologies, Results and Uncertainties, *in Proceedings, GeoRisk 2011: Geotechnical Risk Assessment & Management*, Atlanta, GA, 26-28 June. pp. 845-852.

Cramer, C. H., Gomberg, J. S., Schweig, E. S., Waldron, B. A., and Tucker, K., 2004. The Memphis, Shelby County, Tennessee, Seismic Hazard Maps, U.S. Geol. Surv. Open-File Rept. 2004-1294.

Cramer, C. H., 2006. Quantifying the uncertainty in site amplification modeling and its effects on site-specific seismic-hazard estimation in the upper Mississippi embayment and adjacent areas. *Bull. Seism. Soc. Am* **96(6)**, 2008 - 2020.

Cushing, E.M., Boswell, E.H., and Hosman, R.L, 1964. *General geology of the Mississippi Embayment, Water Resources of Mississippi Embayment*, U.S. Geological Survey Professional Paper 448-B.

Dart, R.L., 1995. *Maps of upper Mississippi Embayment Paleozoic and Precambrian Rocks, U.S. Geologic Survey*, Miscellaneous. Field Study Map, MF-2284, 235 - 249.

Deschenes, M.R., Wood, C.M., Wotherspoon, L.M., Bradley, B.A., and Thomson, E., 2018. Development of Deep Shear Wave Velocity Profiles in the Canterbury Plains, New Zealand, *Earthquake Spectra* **34**, 1065 - 1089.

Dunkin, J.W., 1965. Computation of modal solutions in layered, elastic media at high frequencies, *Bull. Seism. Soc. Am.* **55**, 335–358.

Frankel, A.D., Applegate, D., Tuttle, M.P., and Williams, R.A., 2009. Earthquake hazard in the New Madrid Seismic Zone remains a concern: U.S. Geological Survey Fact Sheet 2009–3071, 2 p.

Foti, S., Comina, C., Boiero, D., 2007. Reliability of combined active and passive surface wave methods. *Italian Geotechnical Journal* **41(2)**, 39 - 47.

Gomberg, J., B. Waldron, E. Schweig, H. Hwang, A. Webbers, R. Van Arsdale, K. Tucker, R. Williams, R. Street, P. Mayne, W. Stephenson, J. Odum, C. Cramer, R. Updike, R. Hutson, and M. Bradley, 2003. Lithology and shear velocity in Memphis, Tennessee, *Bull. Seism. Soc. Am* **93**, 986–997.

Griffiths, S. C., Cox, B. R., Rathje, E. M., and Teague, D. P., 2016b. Mapping dispersion misfit and uncertainty in VS profiles to variability in site response estimates, *Journal of Geotechnical and Geoenvironmental Engineering* **142**(11). doi:10.1061/(ASCE)GT.1943-5606.0001553.

Hashash, M.A., Park, D., 2001. Non-linear one-dimensional seismic ground motion propagation in the Mississippi Embayment, *Engineering Geology* **62**, 185-206.

Hashash, Y., Phillips, C. and Groholski, D., 2010. Recent Advances in Non-Linear Site Response Analysis, in *Proceedings, 5th International Conference on Recent Advances in Geotechnical Earthquake Engineering and Soil Dynamics*, 24 – 29 May, 2010, San Diego, California.

Haskell, N. A., 1953. The dispersion of surface waves on multilayered media, *Bull. Seism. Soc. Am.* **43**, 17–34.

Hosman, R. L., 1996. Regional stratigraphy and subsurface geology of Cenozoic deposits, Gulf Coastal Plain, south-central United States. U.S. Geol. Surv. Profess. Pap. 1416-G, 35

Idriss, I.M. and Akky, M.R., 1979. Primary variables influencing generation of earthquake ground motions by a deconvolution process. Paper No. K 1/3, in *Proceedings, 5th Annual SMiRT Conference*, August 1979.

Knopoff L., 1964. A matrix method for elastic wave problems, *Bull. Seism. Soc. Am.* **54**, 431–438.

Li, W., and Assimaki, D., 2010. Site- and Motion-Dependent Parametric Uncertainty of Site-Response Analyses in Earthquake Simulations, *Bull. Seism. Soc. Am.* **100(3)**, 954–968

Lin, Y. C., Joh, S. H, and Stokoe, K. H., 2014. Analyst J: Analysis of the UTexas 1 Surface Wave Dataset Using the SASW Methodology, Geo-Congress 2014 Technical Papers: Geo-Characterization and Modeling for Sustainability. GSP 234. 2014.

Liu, H. P., Y. Hu, J. Dorman, T.-S. Chang, and J. M. Chiu, 1997. Upper Mississippi Embayment Shallow Seismic Velocities measured in situ, *Eng. Geol*. **46**, 313–330.

Martin, A.J., Shawver, J.B. and Diehl, J.D., 2005. Combined Use of Active and Passive Surface Waves for Cost Effective UBC/IBC Site Classifications, *in Proceedings,* 2005 Annual Meeting on the Association of Environmental and Engineering Geologists.

Mento, D.J., Ervin, C.P., McGinnis, L.D., 1986. Periodic energy release in the New Madrid seismic zone, *Bull. Seism. Soc. Am.* **76**, 1001-1009.

Mayoral, J.M., Asimaki, D., Tepalcapa, S., Wood, C., Roman-de la Sancha, A., Hutchinson, T., Franke, K., Montalva, G., 2019. Site Effects in Mexico City Basin: Past and Present, *Soil Dynamics and Earthquake Engineering* **121 (2019)**, 369-382.

Nanometrics, 2017. *Centaur Products,* Digitizers, http://www.nanometrics.ca/seismology/products/digitizers/centaur.

Park, C.B., Miller, R.D. and Xia, J., 1999. Multichannel analysis of surface waves, *Geophysics* **64(3)**, 800-808.

Park, D. and Hashash, Y., 2005. Evaluation of Seismic Site Factors in the Mississippi Embayment. I. Estimation of Dynamic Properties, *Soil Dynamics and Earthquake Engineering*, **25**, 133 – 144.

Ramírez-Guzmán, L., O., Boyd, S., Hartzell, R., Williams, 2012. Seismic velocity model of the central United States (Version 1): Description and simulation of the 18 April 2008 Mt. Carmel, Illinois, Earthquake, *Bull. Seism. Soc. Am.* **102**, 2622-2645.

Rathje E. M., Kottke A. R. and Trent W. L., 2010. Influence of Input Motion and Site Property Variabilities on Seismic Site Response Analysis, *Journal of Geotechnical and Geoenvironmental Engineering*, **136(4)**, 607- 619.

Redpath, B.B., 1973. Seismic Refraction Exploration for Engineering Site Investigations, Explosive Excavation Research Laboratory, distributed by NTIS.

Redpath, B.B. 2007. "Downhole Measurements of Shear- and Compression Wave Velocities in Boreholes C4993, C4997, C4997 and C4998 at the Waste Treatment Plant DOE Hanford Site". PNNL-16559. Redpath Geophysics, Murphys, California.

Romero, S.M., Rix, G.J., 2005. Ground Motion Amplification of Soil in the Upper Mississippi Embayment. GIT-CEE/GEO-01-1, National Science Foundation Mid America Center, Atlanta.

Rosenblad, B., Bailey, J., Csontos, R. and Van Arsdale, R., 2010. Shear Wave Velocities of Mississippi Embayment Soils from Low Frequency Surface Wave Measurements, *Soil Dynamics and Earthquake Engineering*, **30**, 691 – 701.

Russell, E. E., D. M. Keady, E. A. Mancini, and C. E. Smith, 1982. Upper Cretaceous in the lower Mississippi Embayment of Tennessee and Mississippi: lithostratigraphy and biostratigraphy. Field trip guidebook for the 1982 annual meeting of the Geol. Soc. Am., New Orleans, Louisiana, 40.

Street, R., E. W. Woolery, Z. Wang, and J. B. Harris, 2001. NEHRP soil classifications for estimating site dependent seismic coefficients in the Upper Mississippi Embayment, *Eng. Geol*. **62**, 123–135.

Street, R., and W. Woolery, 2002. Shear-Wave velocities of the postpaleozoic sediments in the Upper Mississippi Embayment, collaborative research between the University of Kentucky and the University of Memphis, U.S. Geol. Surv. Final Tech. Rept., USGS NEHRP Award No. 02HQGR0023, 46 pp.

Teague, D., Cox, B., Bradley, B. and Wotherspoon, L.M., 2015. Development of Realistic Vs Profiles in Christchurch, New Zealand via Active and Ambient Surface Wave Data: Methodologies for Inversion in Complex Interbedded Geology, in *Proceedings, 6th International Conference on Earthquake Geotechnical Engineering*, 1–4 November, 2015, Christchurch, NZ,.

Teague, D., and Cox, B. R., 2016. Site response implications associated with using non-unique V_S profiles from surface wave inversion in comparison with other commonly used methods of accounting for VS uncertainty, *Soil Dynamics and Earthquake Engineering* **91**, 87–103. Available from: http://dx.doi.org/10.1016/j.soildyn.2016.07.028.

Thomson, W. T., 1950. Transmission of elastic waves through a stratified solid medium, *Journal of Applied Physics* **21**, 89–93.

Tokimatsu K, 1997. Geotechnical site characterization using surface waves. In: Ishihara (ed), in *Proceedings, 1st Intl. Conf. Earthquake Geotechnical Engineering* vol 3. Balkema, pp 1333–1368.

Van Arsdale, R.B., TenBrink, R.K., 2000. Late Cretaceous and Cenozoic Geology of the New Madrid Seismic Zone, *Bull. Seism. Soc. Am.* **90**, 345–356.

Wood, C. M. (2009). "The impact of source type, source offset, and receiver spacing on experimental MASW data at soft-over-stiff sites", Thesis, University of Arkansas, 239 pgs.

Wood. C., Ellis, T., Teague, D., & Cox, B., 2014. Analyst I: Comprehensive Analysis of the UTexas1 Surface Wave Dataset, in *Proceedings, ASCE Geo-Congress 2014: Geo-Characterization and Modeling for Sustainability*, 23-26 February, 2014, Atlanta, GA.

Woolery, E.W., Wang, Z., Carpenter, N.S., Street, R. Brengman, C., 2016. The Central United States Seismic Observatory: Site Characterization, Instrumentation, and Recordings, *Seismological Research Letters*, **87(1)**, 215-218.

Zywicki, D.J., 1999. Advanced signal processing methods applied to engineering analysis of seismic surface waves, Ph.D. Dissertation, School of Civil and Environmental Engineering, Georgia Institute of Technology, Atlanta, GA.

Wathelet, M., 2008. An improved neighborhood algorithm: parameter conditions and dynamic scaling, *Geophysical Research Letters* **35**, L09301.

Publications Resulting from This Study

Any future publication resulting from this study would be updated in the following link: **https://doi.org/10.17603/ds2-be10-q668.**

Appendix

DOI of Data

Data collected for this project is freely available through DESIGNSAFE-CI.org at the address below.

https://doi.org/10.17603/ds2-be10-q668.